Sensitivity of Predictions of the Urban Surface Energy Balance and Heat Island to Variations of Urban Canopy Parameters in Simulations with the WRF Model

KODI L. NEMUNAITIS-BERRY

Cooperative Institute for Mesoscale Meteorological Studies, University of Oklahoma, Norman, Oklahoma

PETRA M. KLEIN

School of Meteorology, University of Oklahoma, Norman, Oklahoma

JEFFREY B. BASARA

School of Meteorology, and Oklahoma Climatological Survey, University of Oklahoma, Norman, Oklahoma

EVGENI FEDOROVICH

School of Meteorology, University of Oklahoma, Norman, Oklahoma

(Manuscript received 15 April 2016, in final form 12 November 2016)

ABSTRACT

As NWP and climate models continue to evolve toward finer grid spacing, efforts have been undertaken to better represent urban effects. For this study, the single-layer urban canopy model (SLUCM) of the High-Resolution Land Data Assimilation System (HRLDAS) and WRF Model was used to investigate the sensitivity of near-surface air temperatures and energy fluxes to SLUCM parameters in uncoupled (land) and coupled (land–atmosphere) predictions. Output from HRLDAS and WRF was compared with observations from the Oklahoma Mesonet and Joint Urban 2003 experiment. Variations in roof albedo (0.04–0.4) produced 40–135 W m^{-2} changes in net radiation and sensible heat fluxes. Sensible and ground heat fluxes varied by 40–100 W m^{-2} with changes in roof thermal conductivity (0.05–1.4). The urban fraction was found to be the only SLUCM parameter to significantly impact latent heat fluxes. Near-surface air temperatures, particularly during the daytime, did not show significant variations with SLUCM parameters (remaining within the 0.5-K range). Differences in urban air temperatures due to the change in boundary layer scheme were greater than the temperature changes due to SLUCM parameter variations. The sensitivity of near-surface air temperatures to SLUCM parameters depended on the method used to calculate the skin temperature of the impervious surface. For all simulations, predicted 2-m urban air temperatures were consistently higher than observations, with deviations approaching 8 K during the day and below 3 K at night. These large errors affected the model's skill in reproducing the diurnal cycle of UHI intensity.

1. Introduction

a. Background

To date, much of the current understanding of the impacts of urban areas on atmospheric processes results from field programs conducted in a variety of cities worldwide (Barlow 2014; Loridan and Grimmond 2012), with the majority centered in North American cities: St. Louis, Missouri (Changnon et al. 1971, 1976; Lowry 1974); Chicago, Illinois (Changnon and Semonin 1978; Grimmond and Oke 1995); Los Angeles, California (Grimmond and Oke 1995); Vancouver, British Columbia, Canada (Steyn et al. 1997); Montreal, Quebec, Canada (Mailhot et al. 1998); Mexico City, Mexico (Doran et al. 1998); Tucson, Arizona (Grimmond and Oke 1995); Salt Lake City, Utah (Allwine et al. 2002; Doran et al. 2002); Phoenix, Arizona (Grimmond and Oke 1995; Fast et al. 2000); and Oklahoma City, Oklahoma (Allwine and Flaherty 2006). Because of the complex atmospheric processes occurring in urban areas, field experiments of this nature are critical to scientific advancements in urban meteorology.

While observational studies have long shown that cities significantly impact local weather and climate, the

Corresponding author e-mail: Kodi L. Berry, kodin@ou.edu

DOI: 10.1175/JAMC-D-16-0157.1

prediction of urban effects is a major weakness of current LSMs (Sailor and Fan 2002; Best 2005; Jin et al. 2007). Most LSMs were developed for coarse-resolution atmospheric models in which urban effects were once thought to be negligible (Jin et al. 2007; Oleson et al. 2008). More recent efforts focused on better representation of urbanized areas in NWP and climate models (Masson 2006; Martilli 2007; National Research Council 2012). One common approach is to couple an urban canopy model with an LSM (Masson 2000; Kusaka et al. 2001; Martilli et al. 2002; Wang et al. 2011; Grimmond et al. 2010, 2011). The inclusion of urban meteorological processes and anthropogenic heat release within the LSMs of numerical models is vital for assessing potential impacts of extreme weather events and climate change in heavily populated areas (Betts and Best 2004).

The most documented urban-induced weather phenomenon is the UHI effect whereby surface and air temperatures in the urban canopy are higher than in the rural surroundings (Landsberg 1981; Oke 1987; Arnfield 2003) because of differences in the urban and rural radiation and surface energy balances (SEBs). Urbanized models are often evaluated by comparing predictions of air temperature, surface temperature, wind speed, wind direction, and turbulence statistics with observations (Taha 1999; Martilli et al. 2002; Dupont et al. 2004; Otte et al. 2004; Best 2005; Chin et al. 2005; Fan and Sailor 2005; Grossman-Clarke et al. 2005; Kondo et al. 2005; Holt and Pullen 2007; Lin et al. 2008; Miao et al. 2009; Salamanca et al. 2011; Zhang et al. 2011). However, such evaluations with surface observations do not demonstrate whether the energy exchange processes represented in the urban scheme are physically realistic (Masson et al. 2002; Samuelsson et al. 2003). Thus, several evaluation studies focused on directly comparing the predicted components of the SEB with their observed counterparts (Masson et al. 2002; Lemonsu et al. 2004; Best et al. 2006; Dupont et al. 2006; Grimmond et al. 2010, 2011; Loridan et al. 2010; Loridan and Grimmond 2012; Best and Grimmond 2015). Still, open questions remain about the computation of near-surface (2 m) air temperatures in urbanized weather and climate models (Li and Bou-Zeid 2013, 2014), and evaluation studies should ideally address both predictions of SEB components and atmospheric variables.

The performance of LSMs also depends on whether the model is run in coupled (land–atmosphere) or uncoupled (land) mode because of feedback mechanisms in coupled systems (Margulis and Entekhabi 2001; Samuelsson et al. 2003; Best et al. 2006; Loridan and Grimmond 2012). Several studies used coupled land surface–atmospheric models (Martilli et al. 2002; Dupont et al. 2004; Otte et al. 2004; Best 2005; Chin et al. 2005; Fan and Sailor 2005; Kondo et al. 2005; Liu et al. 2006; Jin et al. 2007; Holt and Pullen 2007; Lin et al. 2008; Lemonsu et al. 2009; Miao et al. 2009; Salamanca et al. 2011; Zhang et al. 2011), which makes it difficult to distinguish the biases of the urban scheme from those of the atmospheric model. Appropriate evaluation of an urban surface scheme must include both uncoupled and coupled model predictions (Best et al. 2006).

The Noah LSM (Ek et al. 2003) has been widely used for UHI studies (e.g., Li and Bou-Zeid 2013, 2014; Hu et al. 2013a) after it was coupled with a single-layer urban canopy model (SLUCM; Chen et al. 2011). It can be run in uncoupled (land) mode using the High-Resolution Land Data Assimilation System (HRLDAS; Chen et al. 2007) for prescribed atmospheric conditions. For coupled predictions that simulate feedback processes between the land surface and the atmosphere that are ignored in HRLDAS, the Noah LSM and SLUCM can be run as part of the WRF Model (Skamarock et al. 2008). Since the HRLDAS and WRF runs use identical parent and nested grids, the SLUCM can be evaluated in both uncoupled and coupled mode.

The performance of the SLUCM depends, in part, on the accuracy of approximately 30 input parameters (Loridan et al. 2010). Some previous studies either used the default values or did not specify whether SLUCM parameter values were modified (Holt and Pullen 2007; Lin et al. 2008; Miao et al. 2009; Tewari et al. 2010; Zhang et al. 2011; Hu et al. 2013a), while some authors adapted the parameter values based on the city of interest (Grossman-Clarke et al. 2010; Flagg and Taylor 2011; Carter et al. 2012; Loridan and Grimmond 2012; Kim et al. 2013). Because of the high level of uncertainty in the specification of SLUCM parameter values, some studies have investigated the sensitivity of a small number of urban parameters using the fully coupled WRF–Noah–SLUCM. For example, Lin et al. (2008) examined the impact of variations of anthropogenic heat flux (Q_F) on the PBL depth and surface air temperature. They also examined the impacts of heat capacity, thermal conductivity, albedo, and roughness length of the roof, building wall, and ground surfaces. Similarly, Miao et al. (2009) conducted four tests by increasing and decreasing building heights and Q_F.

Two studies have implemented complex methods to thoroughly determine the sensitivity of the offline SLUCM to urban parameter values. Loridan et al. (2010) used the Multiobjective Shuffled Complex Evolution Metropolis (MOSCEM) algorithm (Vrugt et al. 2003) to examine the sensitivity of the components of the SEB in the offline SLUCM to variations in the SLUCM and Noah LSM parameters. Wang et al. (2011) used an advanced Monte Carlo simulation tool, subset simulation (Au and Beck 2001), to conduct an analysis of the sensitivity of heat

fluxes and surface temperatures to changes in individual urban canopy parameters in the offline SLUCM. These two studies revealed a strong sensitivity of SLUCM prediction to roof parameters and weak sensitivity to road parameters (Loridan et al. 2010; Wang et al. 2011). The two studies disagreed on the importance of roof, building, and road emissivities. Wang et al. (2011) found that accounting for emissivity of roof, building, and road surfaces had minimal impacts, while Loridan et al. (2010) found that with the roof emissivity, sensible heat flux (Q_H) increased. Urban fraction (f_{urb}) was the only urban parameter to impact latent heat flux (Q_E), as it is handled entirely by the Noah LSM (Loridan et al. 2010).

In summary, much progress has been made over the last decade to develop and evaluate urbanized land surface schemes such as the SLUCM (Chen et al. 2011). However, open questions remain concerning the sensitivity of model predictions to changes in urban parameters and the computation of near-surface variables in atmospheric models like WRF (Loridan and Grimmond 2012; Li and Bou-Zeid 2014). The choice of boundary layer scheme in WRF was also shown to affect the prediction of UHI intensity (Hu et al. 2013a,b).

b. Objectives of the study

The current study is unique in that it tests two different PBL schemes (section 4a), examines the sensitivity to SLUCM parameter changes in both coupled (WRF–Noah–SLUCM; section 4b) and uncoupled (HRLDAS–Noah–SLUCM; section 4c) modes, and investigates the sensitivity of the WRF Model toward different approaches in computing skin temperature (sections 3e and 4d). For this study, the findings of Loridan et al. (2010) and Wang et al. (2011) were used to narrow down the list of the 30 SLUCM parameters to 4: roof albedo (α_{roof}), roof thermal conductivity (k_{roof}), roof width (W_{roof}), and f_{urb}. For Oklahoma City (OKC), coupled and uncoupled predictions with the Noah–SLUCM were obtained using default model parameter values, values more representative of the morphology of OKC (control), and also extreme parameter values (section 3d). The predictions were compared with comprehensive observations of near-surface temperature and components of the SEB that were collected during the Joint Urban experiment in July 2003 (section 2).

2. Data

a. Joint Urban 2003

During June and July 2003, one of the largest urban field experiments, Joint Urban 2003 (JU2003), was conducted in OKC (Clawson et al. 2005; Allwine and Flaherty 2006). Among other factors, OKC was selected as the study area because of the extensive weather-observing infrastructure in central Oklahoma that includes the Oklahoma Mesonet (Brock et al. 1995; Shafer et al. 2000; McPherson et al. 2007), the NOAA/NSSL research polarimetric radar, the NOAA/NWS upper-air station, and four NEXRAD Doppler radars. JU2003 produced perhaps the largest dataset ever compiled to quantify the impact of urban areas on atmospheric processes within the PBL. Between 28 June and 31 July 2003, a vast array of instrument systems, installed specifically for JU2003, collected high-resolution observations of meteorological variables in and around OKC, which were centrally archived (Dugway Proving Ground 2003). The quality assurance (QA) of JU2003 data was performed by the organization that collected the data and by an independent QA contractor (Halvorson et al. 2006).

The Pacific Northwest National Laboratory (PNNL) deployed 32 Onset Computer Corp. ''HOBO Pro Temp/External Temp'' temperature dataloggers (Whiteman et al. 2000) throughout OKC to measure air temperature at 2 m AGL (T_{2m}). HOBOs were deployed along a north–south transect and an east–west transect centered on the central business district (CBD; Fig. 1).

Seven SEB sites were placed across the metropolitan area of OKC (Table 1). The SEB sites were maintained during JU2003 by three organizations: Arizona State University (ASU), NOAA/ARL's Atmospheric Turbulence and Diffusion Division (ATDD), and Indiana University (IU). The sites were located over various land-use types across the city, including suburban lawns, gravel, and concrete. The site locations for the SEB measurements provided data upwind, within, and downwind of downtown OKC (Fig. 2).

b. Oklahoma Mesonet

The Oklahoma Mesonet is an automated network of over 100 remote hydrometeorological stations across Oklahoma (Brock et al. 1995; Shafer et al. 2000; McPherson et al. 2007). Mesonet observations for 10 core variables (including T_{2m}) are collected as 5-min averages, with the exception of soil temperature (15-min averages) and soil moisture (30-min averages).

In 1999, as part of the Oklahoma Atmospheric Surface-Layer Instrumentation System (OASIS) Project, 10 mesonet sites (OASIS supersites) were instrumented to measure the components of the SEB with enhanced accuracy (Brotzge et al. 1999; Brotzge 2000; Basara and Crawford 2002) using, among others, eddy-covariance techniques. Because of their proximity to OKC and availability of data, the OASIS supersite of interest in this study was the Norman, Oklahoma, site (NRMN; Fig. 2).

c. Study period and data processing

To minimize the impacts of varying cloud cover between observation sites and focus on the local urban–atmosphere

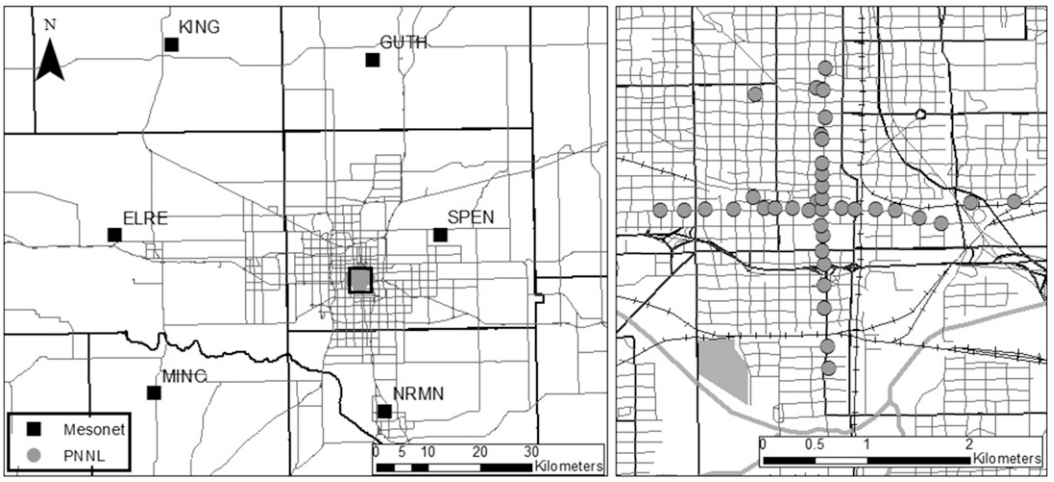

FIG. 1. The locations of the HOBO temperature dataloggers deployed by the PNNL and the Oklahoma Mesonet stations.

interactions, days during JU2003 characterized by strong radiative forcing (solar insolation near theoretical maximum values) and weak wind shear were chosen for this study.

Data from the 32 PNNL HOBO temperature dataloggers and 6 Oklahoma Mesonet sites surrounding the OKC metropolitan area (Fig. 2) were block averaged to hourly values. The mesonet hourly values were then averaged across all six sites to create a mean diurnal cycle of rural T_{2m} (Basara et al. 2008). Similarly, the HOBO hourly values were averaged across all 32 HOBO sites to obtain a mean diurnal cycle of urban T_{2m}. The mean diurnal cycle of the UHI intensity $\Delta T_{u\text{-}r}$ was also calculated.

Data from the OASIS supersites (5-min averages) and ATDD sites (30-min averages) were block averaged to hourly values to reduce the variability of the flux values and ensure consistency across the JU2003 dataset. Mean diurnal cycles were compiled for the following variables: net radiation (Q^*), ground heat flux (Q_G), Q_H, and Q_E. Components of the SEB not directly measured (Q_E at NRMN; Q_G at ATDD gravel, IU TMA, IU TMB, and IU WH) were estimated as the residuals of the SEB equations, when possible. It should be noted that the residual approach allowed any measurement errors in the other terms of the SEB to accumulate in the estimated term. Thus, the residual terms were interpreted as upper limits to the variables estimated.

3. Methodology

The time interval for the case investigated in the current study was 0000 UTC 14 July 2003 to 0000 UTC 16 July 2003. This interval was chosen because it includes two consecutive days where few, if any, clouds were present and the low-level jet was relatively weak (Fast et al. 2005; Hu et al. 2013a).

a. Uncoupled model

NCAR developed HRLDAS (Chen et al. 2007) to initialize the land surface state in WRF coupled model studies. The foundation of the HRLDAS is the Noah LSM, a soil–vegetation–atmosphere transfer scheme initially developed at Oregon State University (Pan and Mahrt 1987). Since then, it has been continuously modified by the NCEP and collaborators for use in the NCEP's regional and global prediction models and data

TABLE 1. SEB sites during the JU2003 field experiment.

Site name	Site description
ATDD gravel	Dirt and gravel parking lot west of the CBD
ATDD concrete	On top of multilevel concrete parking garage in the southwest corner of the CBD
IU TMA	Mounted at ~80 m on booms that extended from radio/cell phone towers owned by the Tyler Media Group
IU TMB	Mounted at ~37 m on booms that extended from radio/cell phone towers owned by the Tyler Media Group
IU WH	Open field north of a residential neighborhood of brick and wood homes
IU GR	North end of the football practice field of a high school
NRMN	Grassy field near the Max Westheimer Airport located 32 km south of the CBD

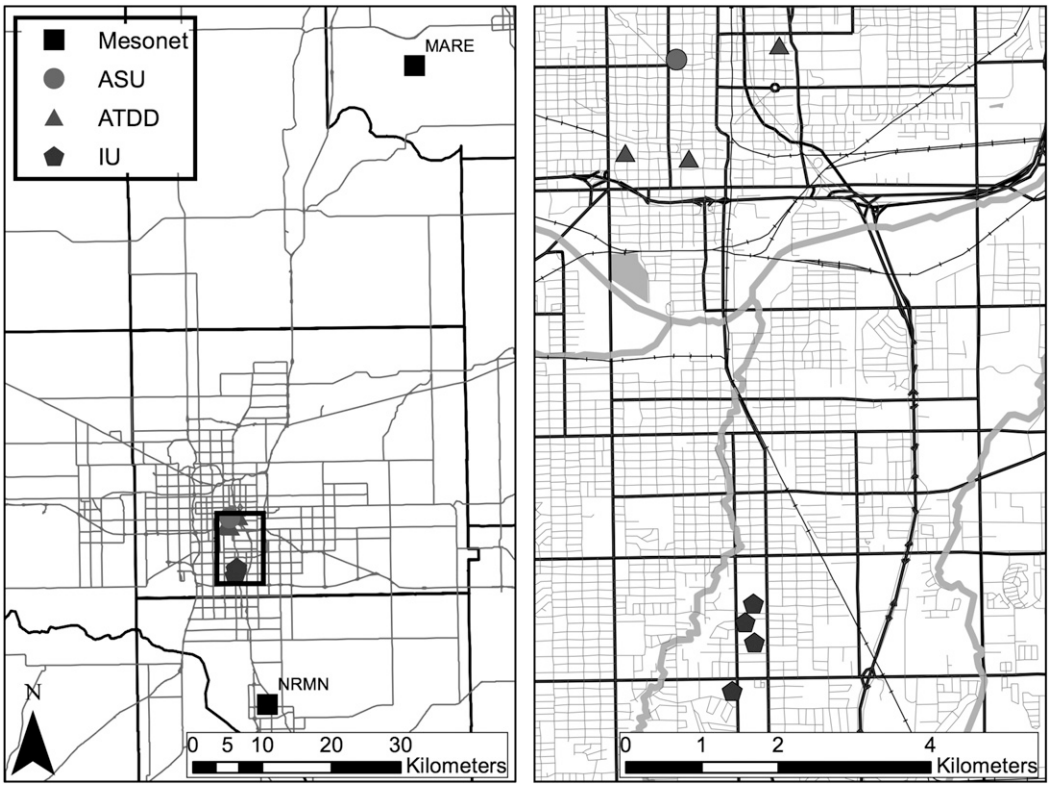

FIG. 2. The locations of the SEB sites deployed by ASU, ATDD, IU, and the Oklahoma Mesonet.

assimilation systems (Chen et al. 1996, 1997; Betts et al. 1997; Koren et al. 1999; Ek et al. 2003). In this study, the HRLDAS is run in an uncoupled mode on the same parent and nested grids as the WRF Model and with the same land-use data, soil texture data, terrain height, vegetation properties, and Noah LSM parameters (Chen et al. 2007). This allows the HRLDAS soil variables (soil moisture and soil temperature) to be directly ingested into the coupled WRF Model without spatial interpolation.

This project used output from the NCEP NARR (Mesinger et al. 2006) to set initial and lateral boundary conditions for the WRF Model and used NARR near-surface atmospheric output for the HRLDAS. The NCEP NARR is a long-term (1979–present) atmospheric and land surface dataset for North America (Mesinger et al. 2006). Because of the project emphasis on the SEB, downward shortwave radiation data from Phase 2 of the North American Land Data Assimilation System (NLDAS-2; Xia et al. 2012) were used for the HRLDAS. The NLDAS-2 uses a ratio-based algorithm to correct the downward shortwave radiation from the NARR to a 5-yr (1996–2000) GOES-retrieved solar radiation (Pinker et al. 2003; Cosgrove and Alonge 2008).

Cosgrove et al. (2003) determined that rough equilibrium with the Noah LSM could be reached within 1 to 2 yr of model run time. This estimate is consistent with the 1.33-yr spinup required to reach rough equilibrium for sandy clay loam soils noted by Chen et al. (2007). Given the multiple years of the NARR forcing data available (1979–2003) prior to the period of interest and results of spinup tests for the study domain (Nemunaitis 2014), the current study opted for the more conservative approach and used a 5-yr spinup time for the HRLDAS. All domains (Fig. 3) were initialized with the NARR output on 1 June 1998. The Noah LSM was run within the HRLDAS using the NARR output and NLDAS-2 solar radiation data through 31 July 2003. A restart file was saved for 5 February 2003 and used to allow each variation in urban parameter to spin up for four months. The HRLDAS output for 0000 UTC for 14 July 2003 replaced the NARR surface states in the WRF input files for each domain. This process ensured that any trends seen in the HRLDAS and WRF Model output were not the result of land surface drift toward model equilibrium.

b. *Coupled model*

The WRF Model is a fully compressible, nonhydrostatic model that utilizes the terrain-following η coordinate and a staggered Arakawa C grid (Skamarock et al. 2008). It allows one-way, two-way, and moving

nesting. In addition, users can choose various subgrid-scale parameterization schemes in seven categories: microphysics, cumulus convection, atmospheric radiation, land surface, surface layer, PBL, and turbulent mixing. The following settings were used in the current study: WRF single-moment 6-class (Dudhia 1989; Hong et al. 1998, 2004; Dudhia et al. 2008) mixed-phase scheme, as mixed-phased schemes should be used for grid sizes less than 10 km (Skamarock et al. 2008); Kain–Fritsch scheme (Kain 2004) for domains with grid spacing larger than 5 km because of its thorough testing within the Eta scheme (Kain 2004); Rapid Radiative Transfer Model (Mlawer et al. 1997) and Dudhia (1989) shortwave radiation scheme, as they have been extensively applied in high-resolution urban WRF studies and allow for a more consistent comparison with prior results for other cities; Yonsei University (YSU; Hong et al. 2006) and MYJ (Mellor and Yamada 1982; Janjić 1990, 1996, 2001) PBL schemes because they are most widely used in conjunction with the SLUCM; MM5 (Paulson 1970; Dyer and Hicks 1970; Webb 1970; Zhang and Anthes 1982; Beljaars 1995) and Eta (Janjić 1996, 2001) surface-layer schemes because they are linked to the MYJ and YSU PBL schemes; and Noah LSM, as it is the only LSM that can be coupled with the SLUCM (Kusaka et al. 2001; Kusaka and Kimura 2004a,b).

Version 3.4.1 of the WRF Model utilized four spatial domains with one-way nesting, 40 vertical levels, and grid spacings of 27, 9, 3, and 1 km (Fig. 3), with the lowest level at approximately 29 m. The HRLDAS used the same four spatial domains. The innermost domain was centered over OKC.

c. SLUCM

A SLUCM is coupled with the Noah LSM within both the HRLDAS and WRF models using a tile approach (Chen et al. 2011). Each urban grid box is assigned an f_{urb} and a fraction of vegetated surface $(1 - f_{\text{urb}})$, which uses grassland as the default vegetated land use. The Noah LSM and SLUCM run separately, and the output fluxes are weighted according to the urbanized fraction of the grid cell (Loridan et al. 2010). The SLUCM represents the f_{urb} as two-dimensional street canyons of infinite length with equal height on both sides (Kusaka et al. 2001; Kusaka and Kimura 2004a; Chen et al. 2006), specified by mean average values of building height (Z_R), street width (W_{road}), and roof width (W_{roof}). The portions of urban surface covered by walls, roads, and roofs are normalized by the total width ($W_{\text{road}} + W_{\text{roof}}$) to determine the contribution each surface type has on the SEB fluxes from the SLUCM.

Within the street canyon, the SLUCM accounts for shadows, reflections, and trapping of radiation. Bulk transfer equations are used to model the Q_H and Q_E above roof surfaces in the SLUCM. The Monin–Obukhov similarity theory is applied to determine the turbulent exchange coefficients above the roof and canyon areas; these coefficients are identical to those calculated by the surface-layer scheme. The Q_H from wall and road surfaces are derived from Jurges's formula (Kusaka et al. 2001). The roof, wall, and road surface temperatures are derived as temperatures that balance the SEBs on the individual canyon surfaces through their effects on Q_H and Q_E.

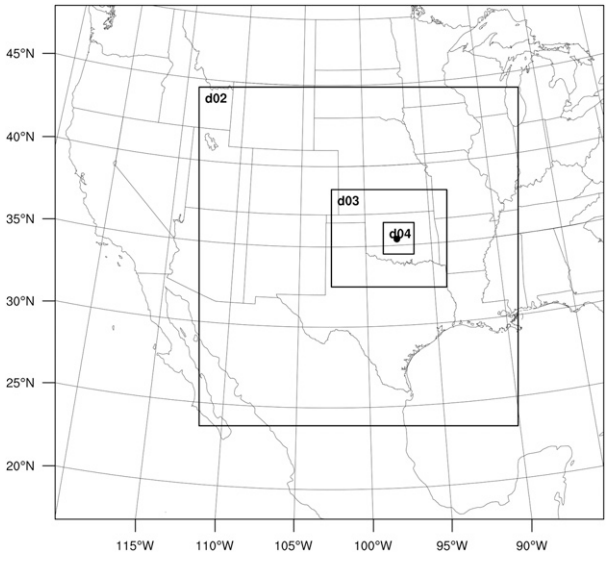

FIG. 3. Domains employed in the WRF and HRLDAS models.

In the WRF–Noah–SLUCM coupling, the SLUCM does not compute the wind profile from the lowest level to the street level, so a logarithmic profile (neutral stability) is assumed from the height of the first model level to the top of the buildings. An exponential profile is used within the urban canyon. A detailed description of the SLUCM implemented in HRLDAS and WRF, including equations and look-up tables, can be found in Loridan et al. (2010).

d. Urban canopy parameters

The urban land-use categories were derived from the National Land Cover Data 2001 (NLCD 2014) and included low-intensity residential (LIR), high-intensity residential (HIR), and industrial/commercial (I/C). Outside of urban areas, the USGS land-use and soil texture data were used.

In version 3.4.1 of the WRF Model, the SLUCM looks up in a table—with three different urban classes (LIR, HIR, and I/C)—approximately 30 input parameters for the thermal properties of the surfaces, dimensions of

TABLE 2. Urban canopy parameter values selected for sensitivity analysis for LIR, HIR, and I/C land-use categories. Boldface numbers indicate values used in the CTL model prediction. The rightmost column lists the related references that motivated the chosen parameter variations. Default refers to the values set as standard values in the SLUCM.

Parameter	LIR	HIR	I/C	Reference
Building height (Z_R)[a]	**4.5**	**8.1**	**8.4**	Burian et al. (2005)
	5.0	7.5	10.0	Default
Standard deviation of building height (σ_z)[a]	**1.8**	**6.2**	**8.9**	Burian et al. (2005)
	1.0	3.0	4.0	Default
Roof width (W_{roof})	8.7	13.4	23.7	
	11.7	**17.4**	**30.7**	Burian et al. (2005)
	14.7	21.4	37.7	
Thermal conductivity of roof (k_{roof})	0.05	0.05	0.05	Roberts et al. (2006)
	0.74	**0.74**	**0.74**	ASHRAE (2009)
	1.40	1.40	1.40	Roberts et al. (2006)
Surface albedo of roof (α_{roof})	0.05	0.05	0.05	Loridan et al. (2010)
	0.20	**0.20**	**0.20**	Default
	0.40	0.40	0.40	Loridan et al. (2010)
Road width (W_{road})	**7.50**	**7.50**	**7.50**	Scott (2006)
Urban fraction (f_{urb})[a]	**0.50**	**0.90**	**0.95**	Default
	0.40	0.50	0.60	

[a] Run with the YSU PBL scheme only.

TABLE 3. Descriptions of the parameter variations for each HRLDAS and WRF Model prediction. For each model run, only the parameters listed below were changed, while for all other parameters the CTL values listed in Table 2 were used.

Model run	Description
aroof_up	α_{roof} set to 0.40 for all urban categories (LIR, HIR, I/C)
aroof_down	α_{roof} set to 0.05 for all urban categories (LIR, HIR, I/C)
kroof_up	k_{roof} set to 1.4 for all urban categories (LIR, HIR, I/C)
kroof_down	k_{roof} set to 0.05 for all urban categories (LIR, HIR, I/C)
Wroof_up	W_{roof} set to 14.7 (LIR), 21.4 (HIR), and 37.7 (I/C)
Wroof_down	W_{roof} set to 8.7 (LIR), 13.4 (HIR), and 23.7 (I/C)
defZR	Z_R set to the default values of 5.0 (LIR), 7.5 (HIR), and 10.0 (I/C)
defZR_SigmaZ	Z_R set to the default values of 5.0 (LIR), 7.5 (HIR), and 10.0 (I/C) σ_z set to the default values of 1.0 (LIR), 3.0 (HIR), and 4.0 (I/C)
defSigmaZ	σ_z set to the default values of 1.0 (LIR), 3.0 (HIR), and 4.0 (I/C)
furb	f_{urb} set to 0.40 (LIR), 0.50 (HIR), and 0.60 (I/C)

canyon geometry, and internal building temperatures (Loridan et al. 2010; Wang et al. 2011).

The current study examines the sensitivity to parameter changes in both coupled (WRF–Noah–SLUCM) and uncoupled (HRLDAS–Noah–SLUCM) modes. The findings of Loridan et al. (2010) and Wang et al. (2011) were used to narrow down the list of SLUCM parameters to investigate. Table 2 lists the parameter values used in the coupled and uncoupled SLUCM predictions for the sensitivity analysis, as well as parameter values that were changed from their default values because of additional data sources specific to OKC. Building height (Z_R) and standard deviation of building height (σ_z) were taken directly from the values derived by Burian et al. (2005) for single-family (single house lots) and multifamily (multiple-unit structures) land-use categories. The I/C values for SLUCM were derived by combining the commercial and services; industrial; transportation, communication, and utility; and the built-up subcategory of the other urban or built-up land-use types (Burian et al. 2005). Roof width (W_{roof}) values for the control run (CTL) were derived from building plan area of Burian et al. (2005) assuming buildings were square shaped.

For the sensitivity studies, roof width values were increased and decreased by 25% in each category from the CTL values, which represent averages for OKC; this accounts for the variability and uncertainty in the original estimates. Data from Scott (2006) were used to convert the average number of lanes for over 55 000 road segments in the OKC metropolitan area to W_{road} using the standard lane width of 3.6 m used by the U.S. Interstate Highway System (Federal Highway Administration 2013). It should be noted that Q_F was neglected in the current study.

The SLUCM parameters were changed one at a time for both the WRF and HRLDAS predictions. Initially, seven model runs were conducted for each of the two PBL schemes. The CTL set of parameter values and naming conventions for the parameter variations relative to the CTL are presented in Tables 2 and 3. Simulations with the Z_R, σ_z, and f_{urb} variations were run with the YSU PBL scheme only. The additional simulations were motivated by the low sensitivity observed in the initial model runs and the differences between the model predictions and observations. We intentionally choose settings that differed significantly from the CTL values to better assess how the model sensitivity compares to the observed errors of the forecasts.

e. Computation of near-surface temperatures

To better explain the response of predicted T_{2m} to variations in urban parameters, the method of calculating the diagnostic T_{2m} within the WRF Model was examined. The 2-m temperature field (T_{2m}) does not affect modeled fields, but is diagnosed from modeled fields and

land surface fields (Jiménez et al. 2012; Li and Bou-Zeid 2014),

$$T_{2m} = T_{skin} - \frac{Q_H}{\rho C_{H2} U_2}, \quad (1)$$

where T_{skin} is the land surface or skin temperature, Q_H is the sensible heat flux at the surface, ρ is the density of air, C_{H2} is the exchange coefficient at 2 m, and U_2 is the wind speed at 2 m.

For urban grid cells when the SLUCM is not used, T_{2m} is calculated according to Eq. (1) using a lookup table for the urban roughness length employed to calculate C_{H2}. When the SLUCM is used, the urban grid cells are divided into impervious and vegetated portions. The vegetated portion of the grid cell is assumed to represent grassland. The assigned fractions of the urban and vegetated portions are based on the f_{urb} specified for each urban land-use category in the urban parameter table. The Noah LSM is called to calculate the T_{skin} for the vegetated fraction. Then the SLUCM is called to calculate the T_{skin} for the impervious fraction. The T_{skin} for the entire grid cell is calculated as a weighted mean of the impervious and vegetated surface temperatures:

$$T_{skin} = T_{skin(SLUCM)} \times f_{urb} + T_{skin(Noah)} \times (1 - f_{urb}). \quad (2)$$

The surface temperature for the impervious portion of the grid is calculated as a diagnostic variable by the SLUCM following

$$T_{skin(SLUCM)} = T_A + \frac{Q_{H(SLUCM)}}{\rho C_H U_A}, \quad (3)$$

where T_A is the air temperature at the lowest model level, while

$$Q_{H(SLUCM)} = Q_{H(roof)} F_{roof} + Q_{H(walls)} F_{walls} + Q_{H(road)} F_{road} \quad (4)$$

is the area-weighted mean of sensible heat fluxes from the roof [$Q_{H(roof)}$], wall [$Q_{H(walls)}$], and road [$Q_{H(road)}$]. The equation for T_{2m} then becomes

$$T_{2m} = T_{skin} - \frac{Q_{H(SLUCM)} f_{urb} + Q_{H(Noah)}(1 - f_{urb})}{\rho C_{H2} U_2}. \quad (5)$$

Li and Bou-Zeid (2014) presented an alternate method to calculate

$$T_{skin(SLUCM)} = T_{roof} F_{roof} + T_{canyon}(1 - F_{roof}), \quad (6)$$

where F_{roof} is the fraction of canyon surface covered by roofs, while T_{roof} and T_{canyon} are the temperatures of the roof and canyon, respectively, which are prognostic variables calculated by the SLUCM. This quantity is similar to the "complete urban surface temperature" proposed by Voogt and Oke (1997), except that the wall and road temperatures are incorporated through the T_{canyon}. A new T_{2m} can be calculated by substituting the $T_{skin(SLUCM)}$ used to calculate T_{skin} in Eq. (5) with that presented by Eq. (6).

4. Results

Validating grid-average model results with instantaneous point-scale observations is a recurring problem. Averaging point-scale observations in time partially remedies this problem by increasing the source area or field of view of the instrument. Because of the heterogeneous nature of urban areas and the relatively small number of SEB sites during JU2003, the observed data were block averaged to hourly values and used primarily to investigate the importance of parameter sensitivity relative to the variability of the observed fields. Because the thermal conductivity of most building materials is higher and the heat capacity is lower than those of rural soils (Landsberg 1981; Oke and Cleugh 1987; Oke 1988), observed values of Q_G were interpreted as lower limits to the modeled values.

The HRLDAS and WRF Model output were extracted for cells that coincided with three or more PNNL HOBO sites, each of the six mesonet sites surrounding OKC, and each of the ASU, ATDD, and IU sites. Data from the PNNL HOBO sites were averaged to represent the observed mean for that grid cell.

a. Air temperature from the WRF Model predictions

Because of the nonlinear interactions between UHIs and heat waves and resulting heat stress for urban residents (Li and Bou-Zeid 2013), it is critical for numerical models (including WRF) to capture the influence of urban land use on the T_{2m}. Figure 4 illustrates the urban and rural T_{2m} predicted by the WRF Model using the MYJ and YSU PBL schemes. Regardless of the PBL scheme used, the WRF Model significantly overestimated T_{2m} during daytime hours for both urban and rural grid points. Except for the overnight hours on 15 July (0000–1200 UTC), variations in the SLUCM parameters produced an approximately 1-K spread of urban temperatures. The spread of predicted urban temperatures increased during the overnight hours of 15 July 2003, during which a decreased k_{roof} and increased f_{urb} produced the largest temperature decreases. The decreased k_{roof} reduced the rate of heat transfer through the top roof layer. As a result, a decrease (increase) in k_{roof} increased (decreased) the amplitude of

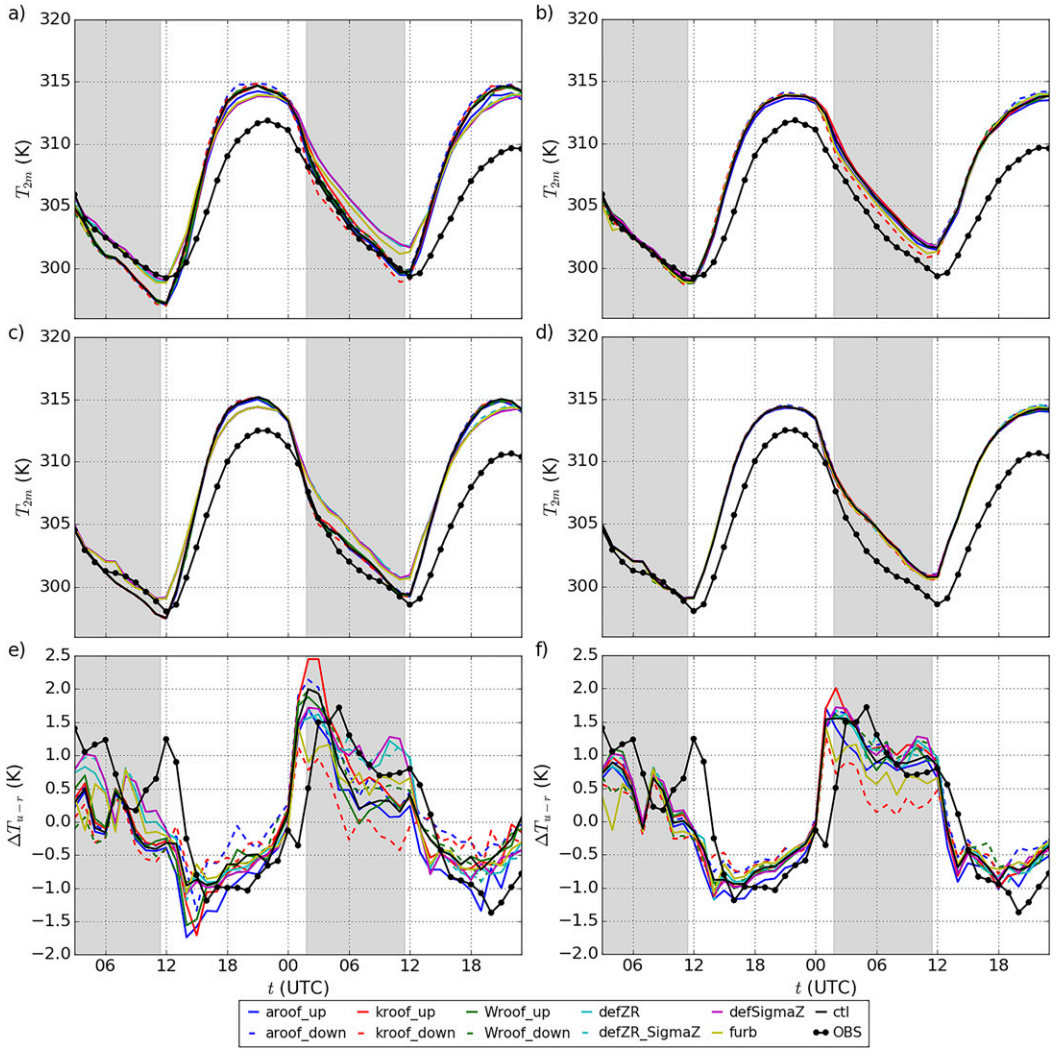

FIG. 4. Diurnal cycles of mean urban temperatures for 14–15 Jul 2003 predicted by the WRF Model using the (a) MYJ and (b) YSU PBL schemes; (c),(d) and (e),(f) as in (a) and (b), but for rural air temperatures and UHI intensity at 2 m, respectively. Observational data from the PNNL HOBO and mesonet sites are shown for comparison. See Table 3 for model run names.

the diurnal cycle of T_{2m}. After sunset, roof temperatures decreased more quickly and contributed to lower nighttime T_{2m}. The decreased f_{urb} shrank the fraction of the grid cell composed of urban surface and increased the vegetated fraction, resulting in decreased nighttime temperatures. During the daytime hours, the decrease (increase) in α_{roof} increased (decreased) the T_{2m} because of the resulting increase (decrease) in energy available to heat the roof surface. However, differences in urban T_{2m} due to the change in PBL scheme were greater than the temperature changes due to urban parameter variations. The changes in the predicted rural temperatures may be attributed to the NRMN grid cell being classified as LIR land use in the NLCD 2001.

The MYJ PBL scheme produced a larger amplitude of the diurnal cycle than the YSU scheme. As a result, nighttime urban T_{2m} predicted using the MYJ scheme compared well to the observed temperatures. However, the daytime predicted temperatures were 2–5 K greater than observed. The temperatures predicted when using the YSU scheme were consistently 1–3 K higher than the observed temperatures for all hours.

After the initial analysis of the sensitivity of the T_{2m} to variations in the α_{roof}, k_{roof}, and W_{roof}, additional model runs were conducted using only the YSU PBL scheme. The considered variations of SLUCM parameters included decreasing the f_{urb} (discussed above), using the default values for σ_z, using the default values for Z_R, and

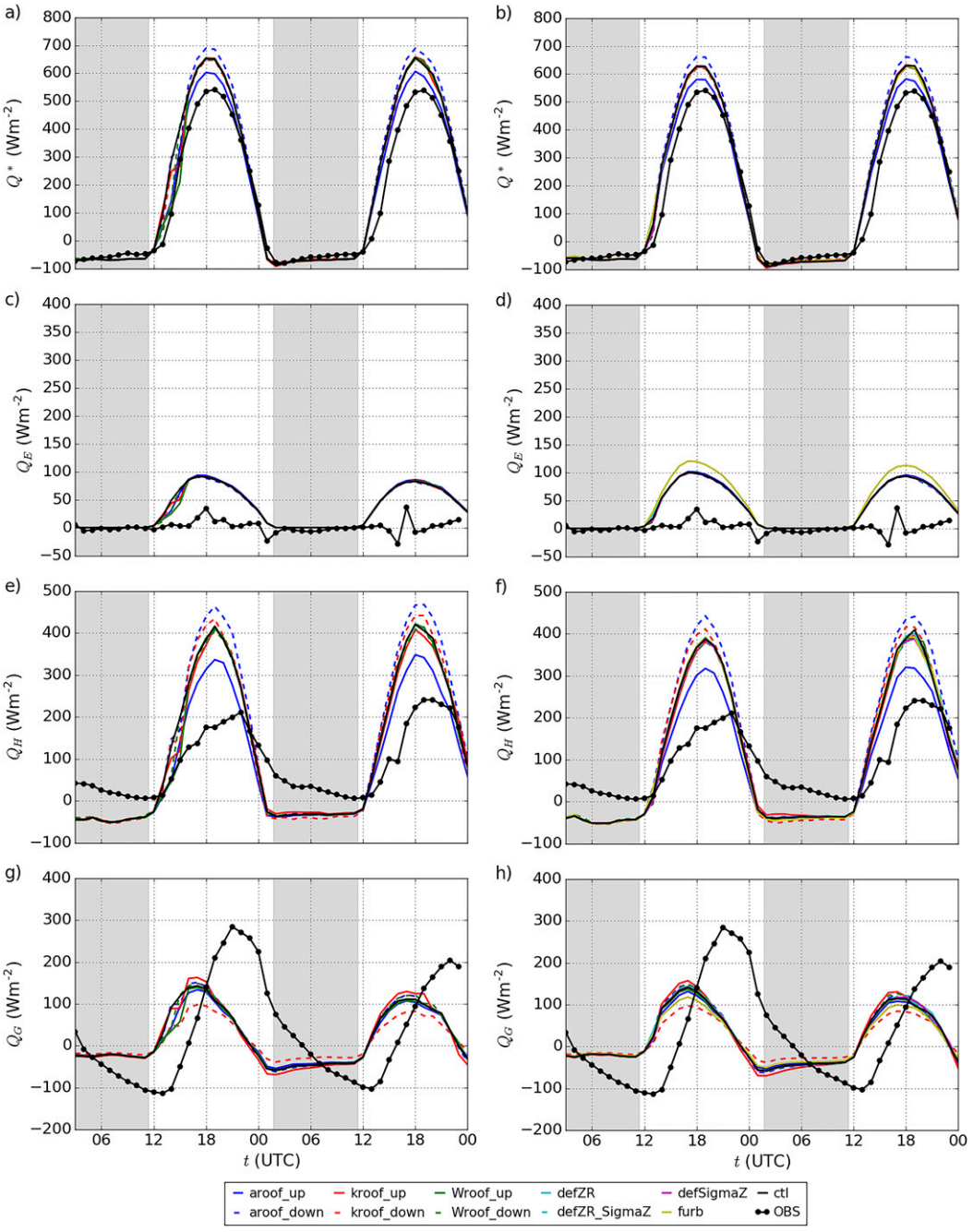

FIG. 5. As in Fig. 4, but for (a),(b) Q^*, (c),(d) Q_E, (e),(f) Q_H, and (g),(h) Q_G and with observational data from the ATDD concrete site (LIR).

using the default values for both σ_z and Z_R. Varying Z_R and σ_z did not significantly impact the T_{2m}.

Figures 4e and 4f display the predicted difference between urban and rural temperatures, or UHI intensity ($\Delta T_{u\text{-}r}$), for each parameter variation using both PBL schemes. The $\Delta T_{u\text{-}r}$ values predicted with both PBL schemes, regardless of the parameter variations, were consistent with the $\Delta T_{u\text{-}r}$ observed, but only because both the predicted urban and rural temperatures at 2 m exhibited the same trends. The diurnal cycle of $\Delta T_{u\text{-}r}$ predicted by the WRF Model peaked 1–2 h earlier than the observed $\Delta T_{u\text{-}r}$ because of rapid rural cooling at sunset.

The sensitivity of H_{SLUCM} [Eqs. (3) and (5)], Q_H [Eq. (1)], and other components of the SEB to variations in urban canopy parameters were further examined to

TABLE 4. Mean maximum daytime (nighttime) differences in heat fluxes ($W\,m^{-2}$) between model runs varying urban parameters and the CTL run.

			α_{roof_up}	α_{roof_down}	k_{roof_up}	k_{roof_down}	f_{urb}
Q^*	LIR	WRF	−52	38	4 (−6)	−8 (8)	—
	I/C	WRF	−136	99	7 (−8)	−15 (11)	—
Q_E	LIR	WRF	8	−6	—	—	25
		HRLDAS		−3	—	—	11
	I/C	WRF	—	—	—	—	78
		HRLDAS	—	—	—	—	36
Q_H	LIR	WRF	−83	56	−15 (9)	24 (−14)	6 (−10)
		HRLDAS	−69	52	−15 (11)	32 (−19)	17 (−10)
	I/C	WRF	−130	89	−38 (24)	78 (−36)	9 (−35)
		HRLDAS	−107	81	−35 (27)	80 (−47)	56 (−32)
Q_G	LIR	WRF	−12 (7)	11 (−6)	18 (−12)	−40 (21)	−20 (11)
		HRLDAS	−8 (6)	6 (−5)	18 (−14)	−40 (27)	−20 (15)
	I/C	WRF	−25 (17)	21 (−14)	45 (−32)	−100 (51)	−64 (35)
		HRLDAS	−20 (17)	14 (−11)	46 (−36)	−101 (68)	−63 (49)

understand the lack of response of predicted 2-m temperatures.

b. *Components of the surface energy balance from the WRF Model predictions*

Figure 5 illustrates the Q^*, Q_E, Q_H, and Q_G predicted by the WRF Model using the MYJ and YSU PBL schemes for the grid cell containing the ATDD concrete site. All components of the SEB responded similarly to changes in the urban parameters, regardless of the PBL scheme used. Examination of cloud fraction and downwelling shortwave radiation (not shown) revealed minor differences in predicted cloud cover associated with a stationary front moving southeast across the domain, evident between 1300 and 1600 UTC 14 July 2003 in all components of the SEB. Aside from differences in early morning clouds, the magnitudes of all components of the SEB with the MYJ scheme were typically within $40\,W\,m^{-2}$ from respective component magnitudes calculated with the YSU scheme. Because of the consistency in response to variations in urban parameters for each grid cell examined, the discussion forward will primarily focus on the YSU results.

Table 4 summarizes the average largest daytime and nighttime differences in components of the SEB between sensitivity runs and the CTL. The land uses for the grid cells containing the ATDD concrete and ATDD gravel sites were LIR and I/C, respectively (Fig. 6). Varying the f_{urb} caused larger variations in the fluxes for the I/C than LIR land use, which agrees with the more drastic change in f_{urb} tested for I/C. Consistent across all grid cells examined (see Figs. 7 and 8 and Table 4), α_{roof} was the only SLUCM parameter that significantly impacted Q^* (Wang et al. 2011; Loridan et al. 2010).

The predicted daytime values of Q_E for the grid cell containing the ATDD gravel site (I/C) were 100–150 $W\,m^{-2}$ less than the predicted Q_E values for the LIR grid cells (Figs. 5 and 6). Consistent with Loridan et al. (2010), the only urban parameter to significantly impact Q_E was f_{urb}. The value of Q_E was only sensitive to f_{urb} because the SLUCM predicted values of Q_E equal to $0\,W\,m^{-2}$ for the entire forecast period (Loridan et al. 2010). The f_{urb} simply increased the percentage of Q_E predicted by the Noah LSM that contributed to the calculation. All other parameter variations impacted Q_E by less than $10\,W\,m^{-2}$.

The urban parameter variations that most significantly impacted Q_H were variations of α_{roof} and k_{roof}. As stated previously, because of the larger associated f_{urb}, the Q_H for the grid cell with I/C land use (ATDD gravel; Fig. 6) varied more with parameter changes than Q_H for the LIR grid cells (Figs. 5, 7, and 8; Table 4). The α_{roof} impacted Q_H through altering the amount of energy (Q^*) available to heat the roof surface. The decrease (increase) in k_{roof} decreased (increased) the transfer of heat through the roof layer and resulted in higher (lower) roof surface temperatures and Q_H (Loridan et al. 2010).

The SLUCM parameters that impacted Q_G the most were k_{roof} and f_{urb}. The value of Q_G is directly proportional to k_{roof}, as it controls the transfer of heat through the roof surface. An increase (decrease) in k_{roof} resulted in an increased (decreased) amplitude of the diurnal cycle of Q_G. During the day, the increased (decreased) k_{roof} increased (decreased) the transfer of heat to the roof in comparison with the CTL (Figs. 5–8; Table 4). At night, the transfer of heat toward the surface of the roof was increased (decreased). The values of Q_G predicted by the SLUCM were higher than those predicted by the Noah LSM. The decrease in f_{urb} decreased the SLUCM contribution to the gridcell Q_G.

Overall, observations collected above mean building height (TMA, TMB) or away from buildings compared

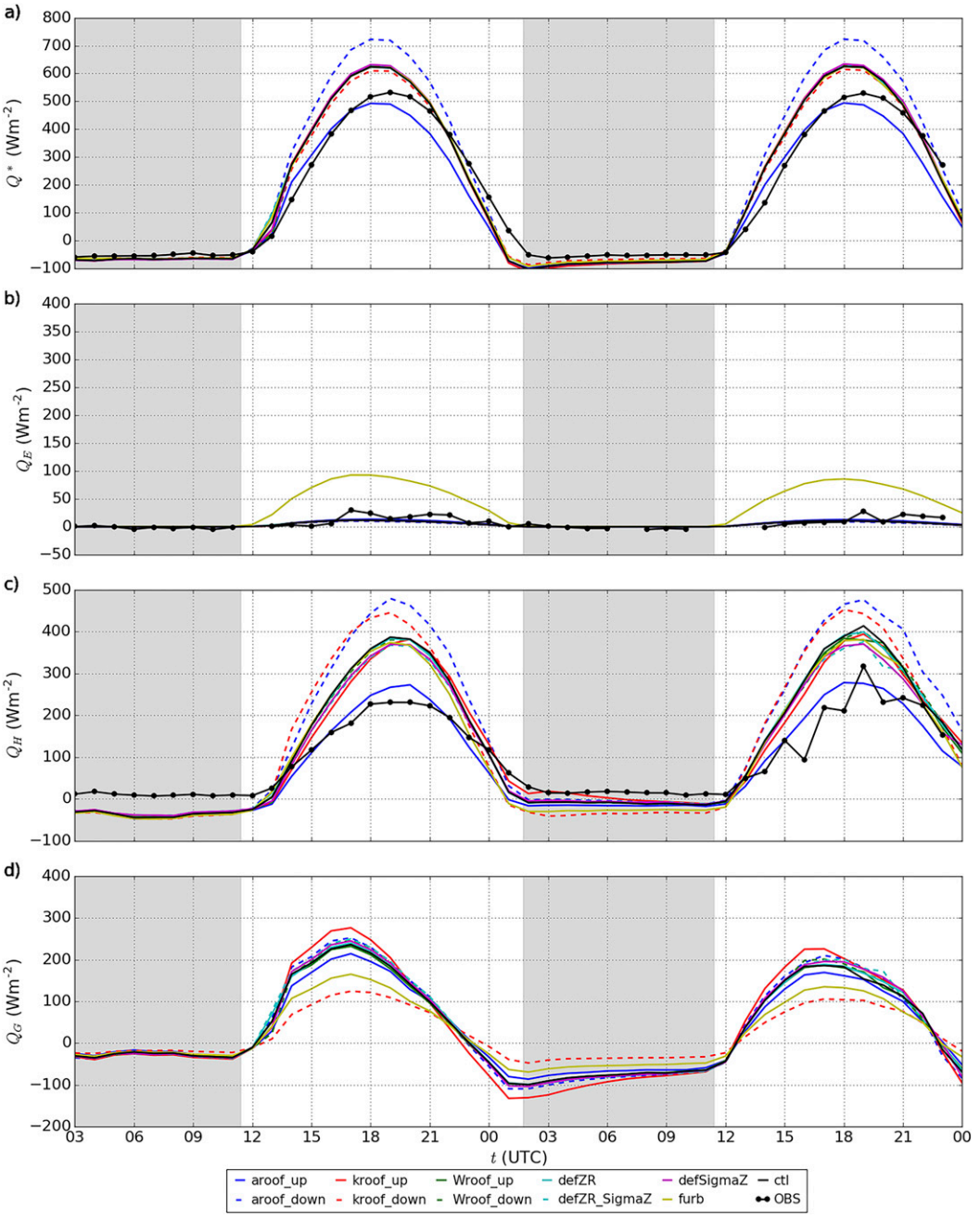

FIG. 6. As in Fig. 4, but for only (a) Q^*, (b) Q_E, (c) Q_H, and (d) Q_G predicted by the WRF Model using the YSU PBL scheme and with observational data from the ATDD gravel site (I/C).

more favorably to modeled values than did observations collected within the urban canopy layer. When compared with the observations from the SEB sites, predicted values of Q^* either were 50–100 W m^{-2} greater than the observed values (ATDD concrete, ATDD gravel, and IU GR) or compared favorably to observations (IU TMA, IU TMB, IU WH, and NRMN). Values of Q_E observed at the ATDD concrete site were significantly smaller than those predicted by the WRF Model because this site was the most urbanized site, while the land-cover category for the grid cell containing that site was LIR. Except for the ATDD gravel site, the predicted LIR Q_E values were significantly lower than observed values, likely because of site proximity to suburban neighborhoods with lawn irrigation. Even at the ATDD sites, observed Q_H values were 100–150 W m^{-2}

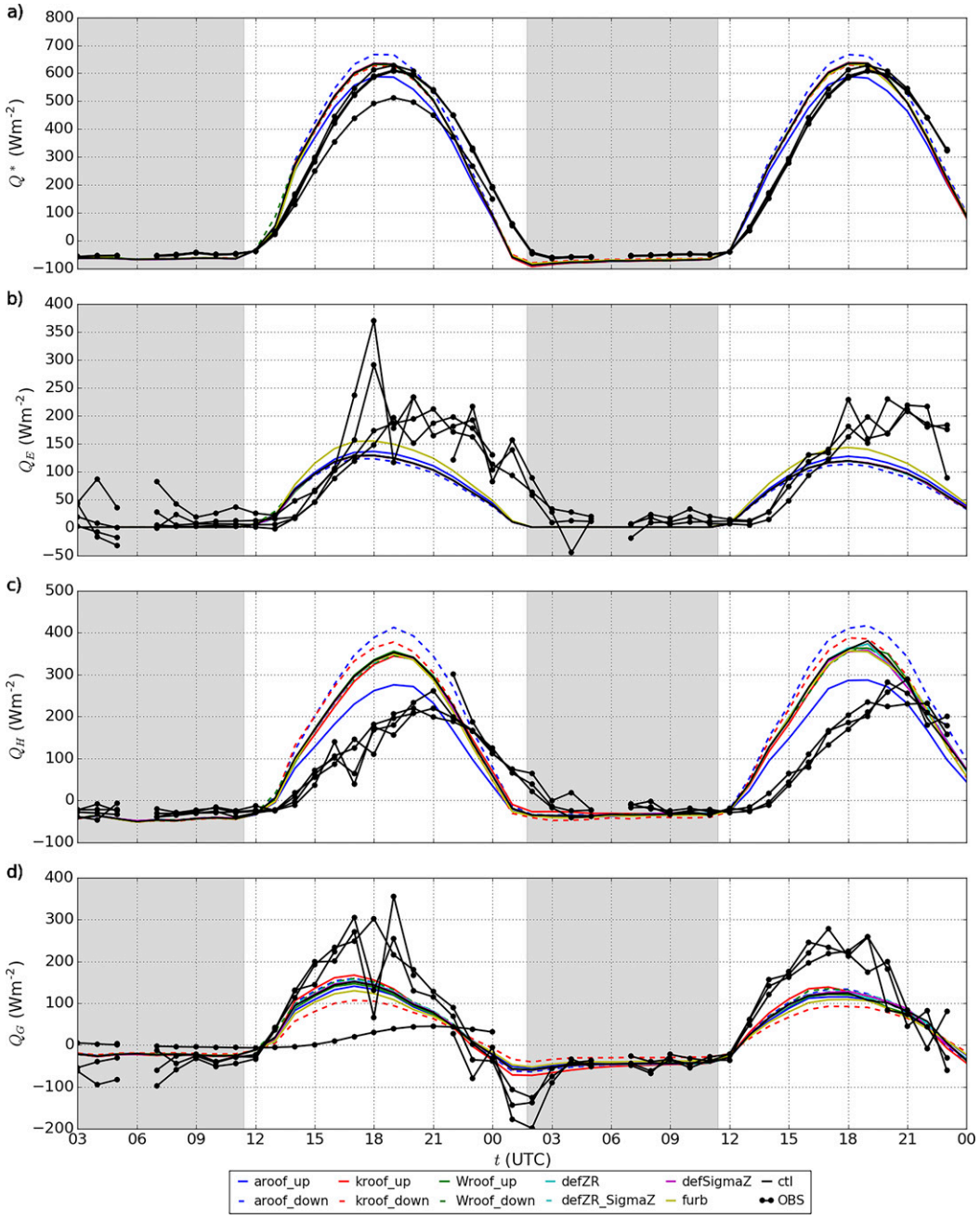

FIG. 7. As in Fig.6, but with observational data from the IU GR, TMA, TMB, and WH sites (LIR). The same symbol is used for all four sites to highlight the variability among the three sites, not to describe specific details of individual sites.

smaller than the predicted values. However, observed Q_H values remained positive overnight at the two ATDD sites, while the WRF Model failed to maintain positive Q_H during nighttime hours. Positive Q_H at night is considered a significant contributor to the development of the UHI (Yap and Oke 1974; Kalanda et al. 1980; Oke 1988; Grimmond and Oke 1995; Grimmond et al. 2004; Offerle et al. 2006). Finally, the diurnal cycle of Q_G predicted by the WRF Model consistently peaked earlier than the observed diurnal cycle.

c. *Components of the surface energy balance from HRLDAS predictions*

The current study also looked at the impact of running the Noah–SLUCM within the HRLDAS in an uncoupled

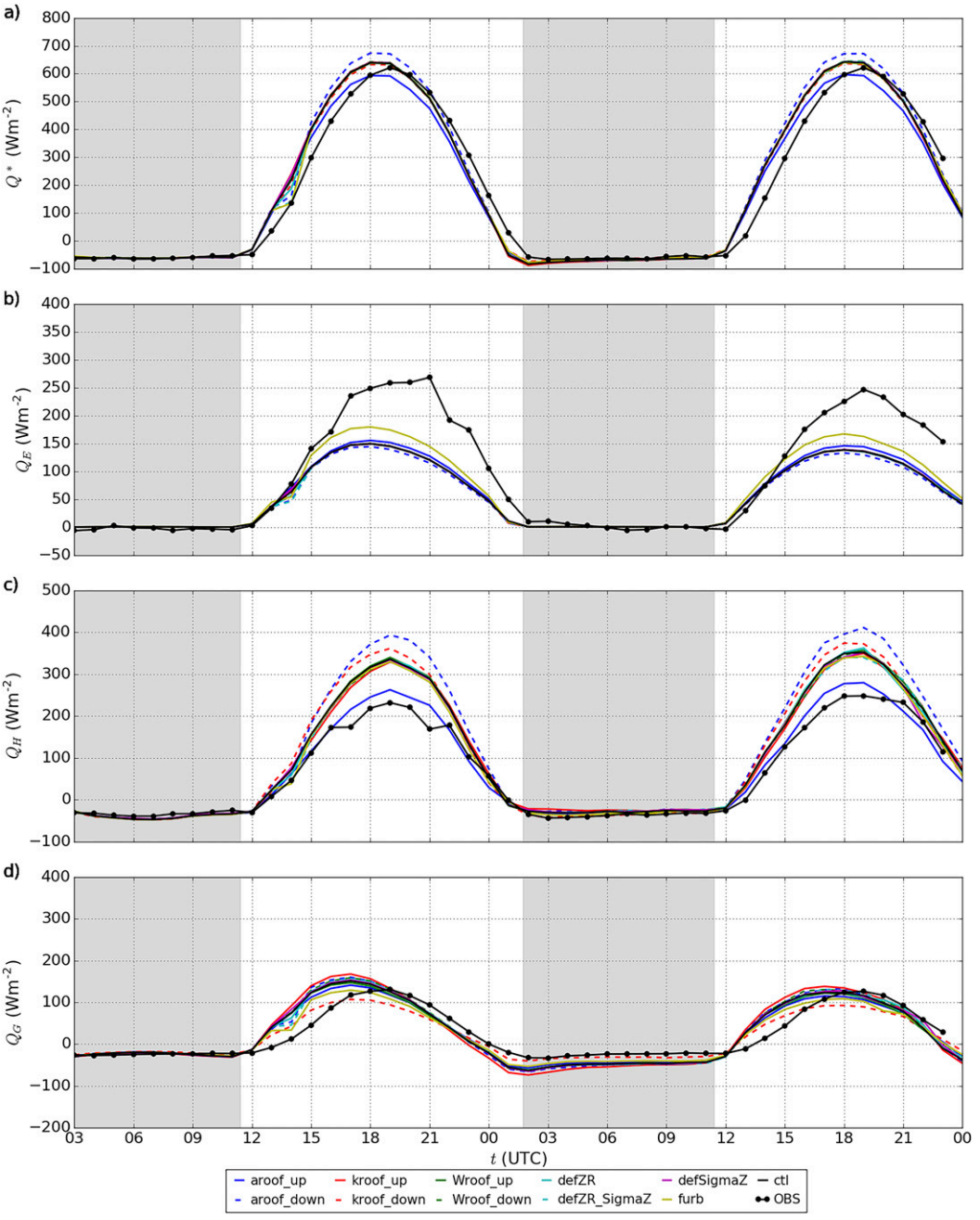

FIG. 8. As in Fig.6, but with observational data from the NRMN site (LIR).

mode (Table 4) to test if the fluxes were more responsive to changes in the SLUCM parameters without the WRF Model feedback mechanisms (Best et al. 2006). While the sensitivity to SLUCM variations was similar between the WRF and HRLDAS predictions, the flux magnitudes differed significantly.

It was not possible to calculate Q^* values from the HRLDAS input and output data as the calculated emissivity was not included in the HRLDAS output files. Values of Q_E predicted by the HRLDAS for all urban land-use types were 50–75 W m^{-2} smaller than values of Q_E predicted by the WRF Model for all parameter variations (Figs. 9–12). Values of Q_H predicted by the HRLDAS for LIR grid cells (all except ATDD gravel) were approximately 25–75 W m^{-2} greater than values of Q_H predicted by all WRF Model runs (Figs. 9–12). Values of Q_H predicted by the HRLDAS for the I/C grid cell (ATDD gravel) were slightly less than

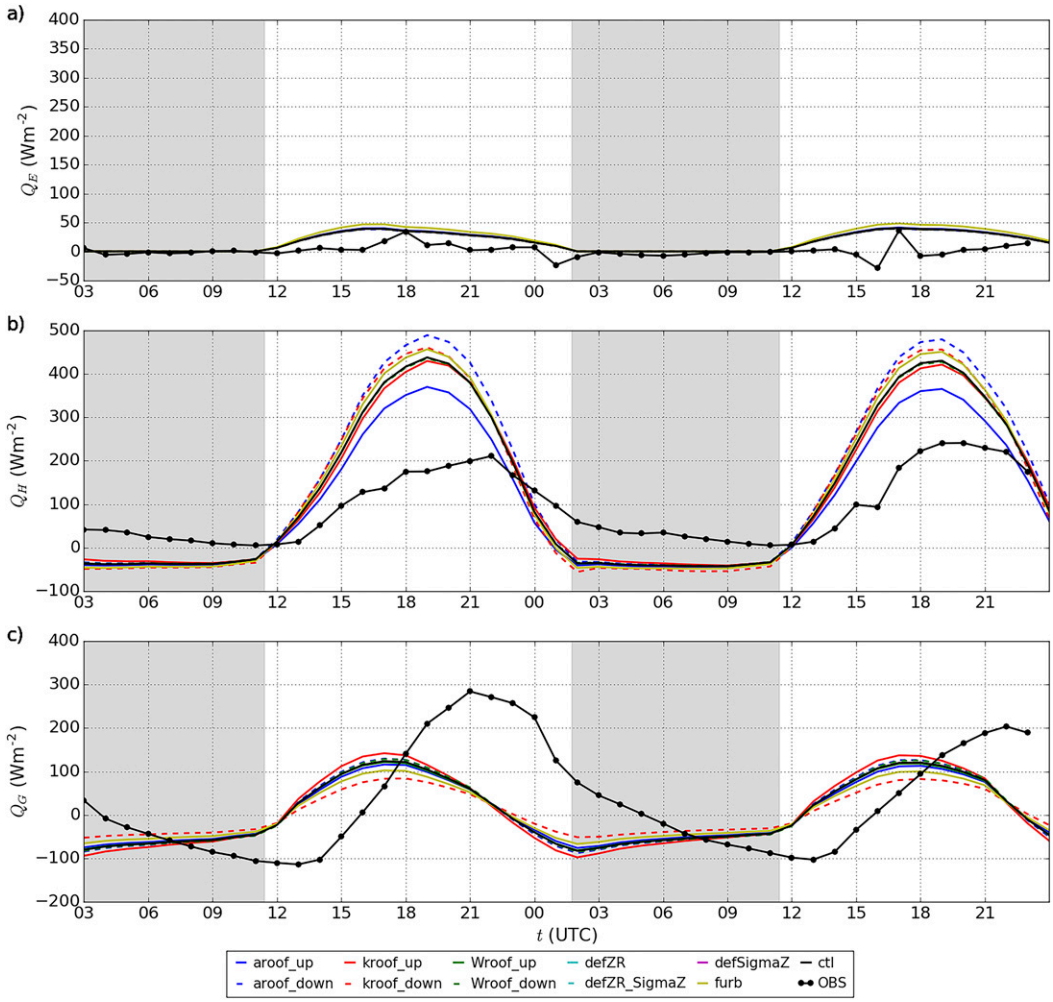

FIG. 9. As in Fig. 4, but predicted by the HRLDAS and with observational data from the ATDD concrete site (LIR).

Q_H predicted by the WRF Model for all parameter variations (Figs. 9–12). Values of Q_G predicted by the HRLDAS were approximately 25 W m^{-2} greater than those predicted by the WRF Model (Figs. 9–12). The responses of the fluxes to changes in the urban canopy parameters were nearly the same when SLUCM was run in an uncoupled mode with the HRLDAS as compared with coupled mode with the WRF Model. Notable exceptions were the sensitivities of Q_E and Q_H to f_{urb} (Table 4). Values of Q_E predicted by the HRLDAS were less sensitive to urban fraction than predicted by the WRF Model. For I/C land use (ATDD gravel), the decrease in f_{urb} from 0.95 to 0.6 resulted in peak Q_E values of 50 W m^{-2} predicted by the HRLDAS and 100 W m^{-2} predicted by the WRF Model. Changes in the W_{roof}, Z_R, and σ_z did not significantly impact the components of the SEB in both uncoupled and coupled land–atmospheric systems. However, the lack of response of $T_{2\text{m}}$ to changes in urban parameters was found to be not associated with a lack of response in Q_H. This led to the investigation of the sensitivity of T_{skin} to changes in SLUCM parameters.

d. *Skin and near-surface temperatures from the WRF Model predictions*

Figure 13a shows urban T_{skin} predicted by the WRF Model using the YSU PBL scheme. In contrast to $T_{2\text{m}}$ (shown in Fig. 4), changes in SLUCM parameters produced noticeable changes in predicted T_{skin} during both daytime and nighttime hours. The value of T_{skin} was most sensitive during the daytime to increases (decreases) in α_{roof}. Predicted decreases (increases) in T_{skin} were in the range from 1 to 2 K as α_{roof} altered the amount of energy available for heating the roof surface. The decrease in k_{roof} increased T_{skin} by 1K during the daytime because of the reduced transfer of heat through the roof layer. The quantity k_{roof} was the most impactful factor during the night, resulting in a 2-K decrease in T_{skin}. After sunset, the decreased k_{roof} resulted in more

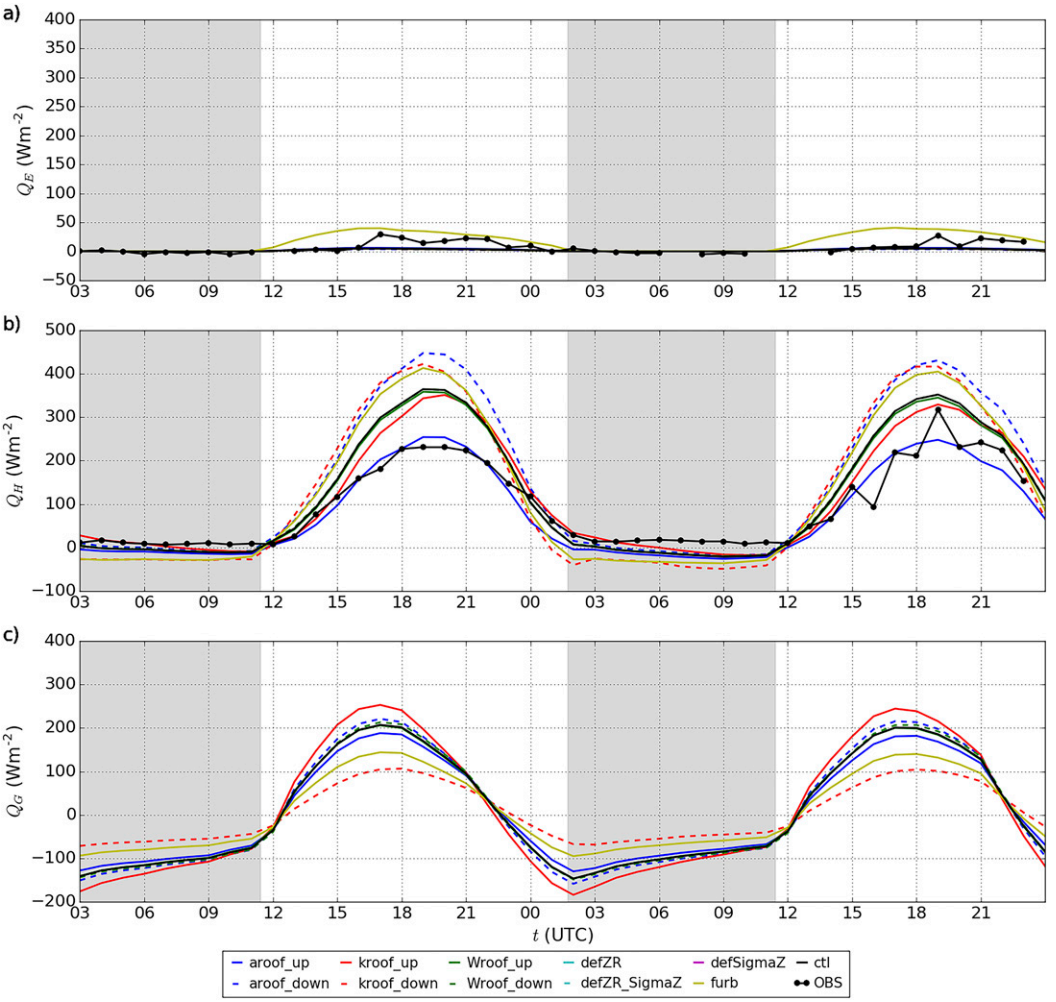

FIG. 10. As in Fig. 9, but with observational data from the ATDD gravel site (I/C).

rapid cooling of the roof surface and reduced transfer of heat toward the surface of the roof. In contrast, when the k_{roof} was increased, nighttime values of T_{skin} increased because of the increased upward transfer of heat through the roof surface.

While the sensitivity of T_{skin} was greater than the sensitivity of 2-m temperature to changes in SLUCM parameters, it was surprising that large changes in Q_H (up to 120 W m^{-2}) resulted in modest changes in T_{skin} (1–2 K). Recalling how the WRF Model calculates $T_{\text{skin(SLUCM)}}$, Eq. (3) is only correct if the C_H contains roughness lengths for the impervious surfaces (Li and Bou-Zeid 2014). In version 3.4.1 of the WRF Model, the C_H used for the urban grid cell was calculated based on the roughness lengths of the vegetated grassland surface as opposed to roughness lengths appropriate for urban land use. This inconsistency in roughness lengths does not capture the bulk influence of the impervious fraction and causes the reduced sensitivity of $T_{2\text{m}}$ to changes in SLUCM parameters. The default calculation of $T_{2\text{m}}$ (using C_{H2} for grassland at 2 m) appears to be adequate because $T_{2\text{m}}$ is less sensitive to C_{H2} than the T_{skin} and is not truly representative of the air temperature at 2 m because of the complexity of the urban surface (Li and Bou-Zeid 2014).

Figures 13b–d illustrate the T_{skin}, $T_{2\text{m}}$, and $\Delta T_{u\text{-}r}$ for urban grid cells resulting from implementation of Eq. (6) in the SLUCM. The method for calculating $T_{\text{skin(SLUCM)}}$ led to a 1–3-K increase in T_{skin} during the day for all parameter variations relative to the original method. Except for decreased T_{skin} at night when the k_{roof} was decreased, the nighttime spread of predicted T_{skin} with variations in urban parameters did not change with the use of Eq. (6). Variations in W_{roof} and f_{urb} still resulted in very small (<1 K) changes of T_{skin} relative to the CTL.

Daytime values of $T_{2\text{m}}$ were higher because of larger values of T_{skin} calculated using Eq. (6). Nighttime values of $T_{2\text{m}}$ were consistent with trends in T_{skin} and the originally calculated $T_{2\text{m}}$. The quantity k_{roof} was the only

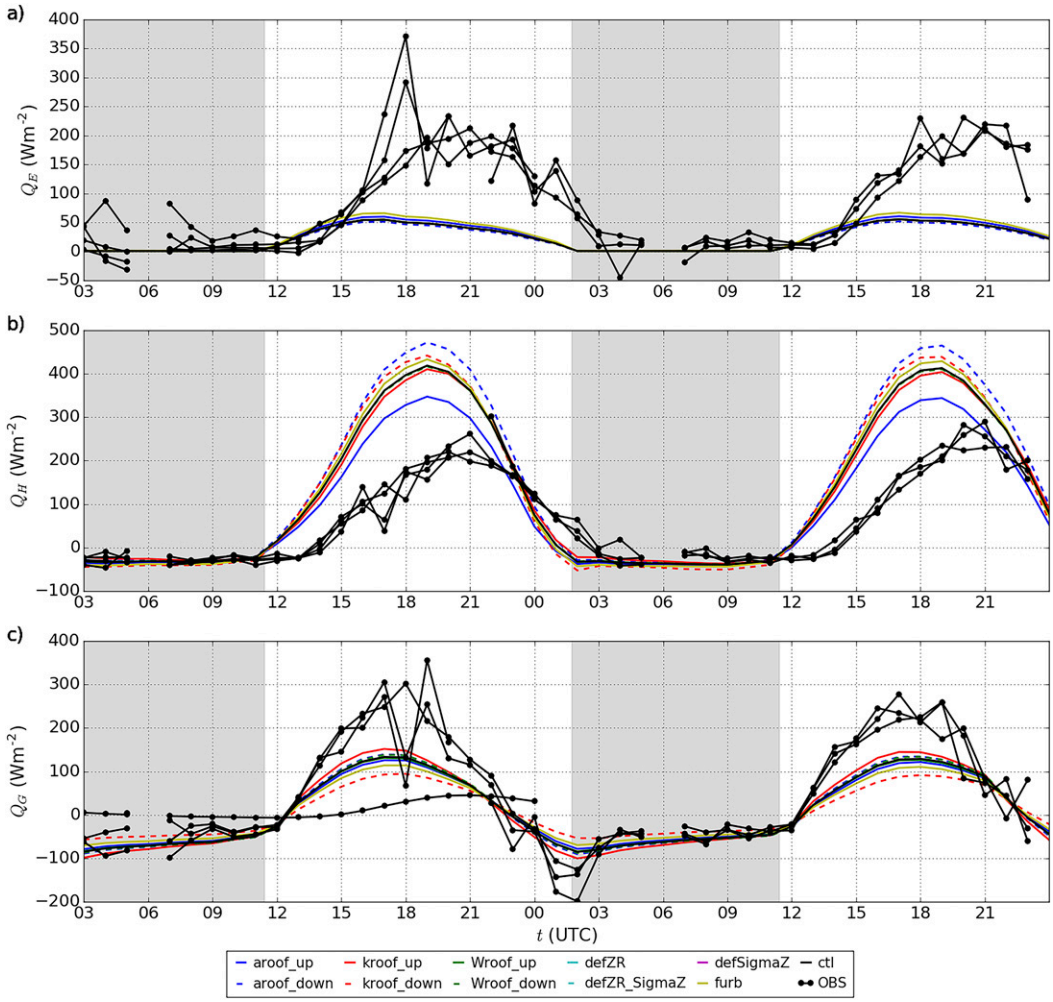

FIG. 11. As in Fig. 9, but with observational data from the IU GR, TMA, TMB, and WH sites (LIR).

urban parameter to which nighttime T_{2m} were sensitive. Despite none of the components of the SEB being sensitive to the W_{roof} when combined with the new formulation for $T_{skin(SLUCM)}$, the values of T_{2m} were most sensitive to increased W_{roof} and decreased α_{roof} during the daytime and decreased k_{roof} at all hours of the day. The higher sensitivity of T_{2m} to W_{roof} was due to W_{roof} being used directly in the calculation of $T_{skin(SLUCM)}$ combined with the lack of response of Q_H to W_{roof}. Because T_{2m} is a function of the difference between T_{skin} and Q_H, a slight sensitivity of T_{skin} to W_{roof} and a lack of sensitivity of Q_H to W_{roof} produced a T_{2m} sensitive to W_{roof}. The higher sensitivity of T_{2m} to f_{urb} was similar to that of W_{roof}.

Implementing Eq. (6) in the SLUCM increased the sensitivity of T_{2m} to urban canopy parameters, especially during the daytime. However, its implementation also increased the daytime UHI intensity, increased the disparity between observed and predicted daytime temperatures, and failed to improve the temporal difference. While the observations show a daytime cool island developing with urban temperatures 1°C cooler than surrounding rural temperatures, the WRF Model predicts a daytime heat island ranging from 1° to 2.5°C. Depending on the choice of urban parameters, the predicted daytime UHI intensity is higher than the nighttime UHI intensity, which was never observed during JU2003 and is generally rarely observed. Because of the sensitivity of T_{2m} to the method of calculating T_{skin}, additional cases and approaches to calculate T_{skin}, the sensitivity of temperatures at higher levels, and temporal differences should be investigated.

5. Summary and conclusions

This study investigated changes in the surface energy and radiation balances that contribute the development

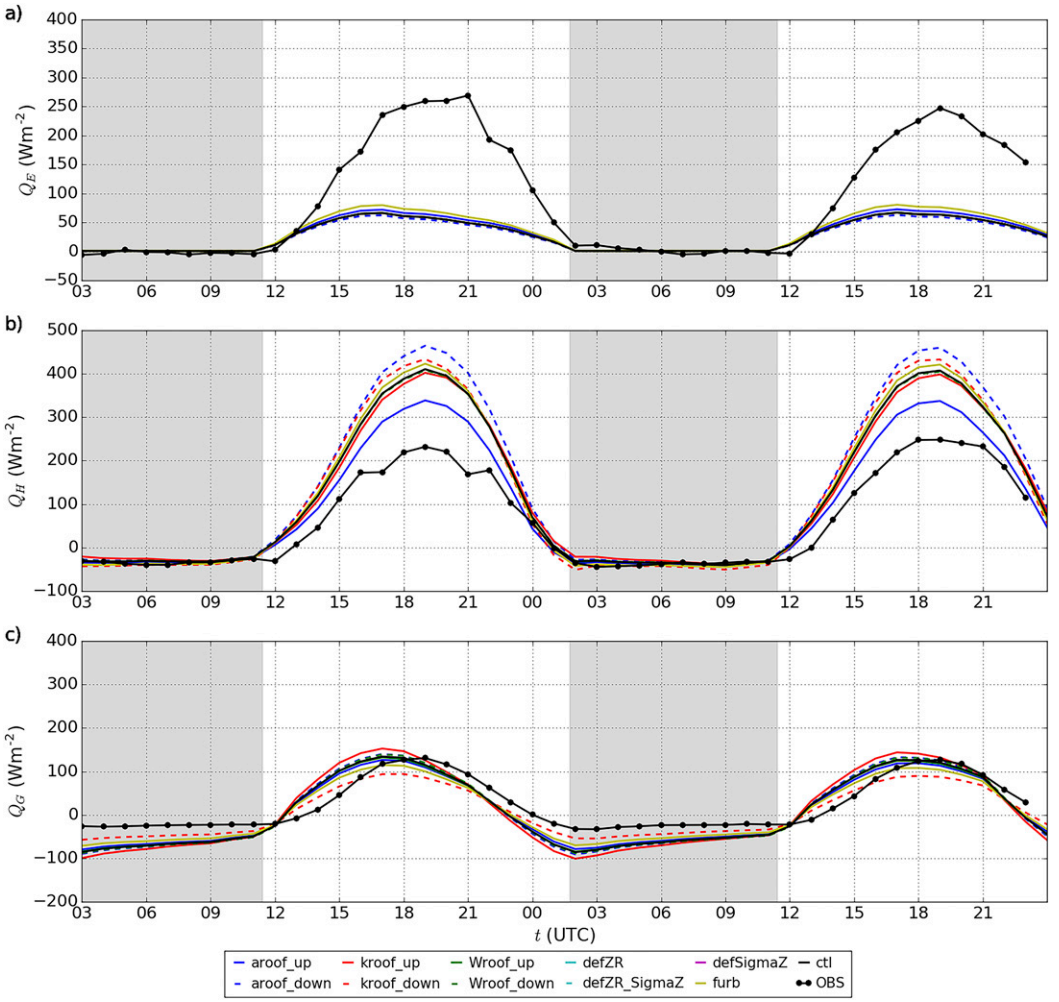

FIG. 12. As in Fig. 9, but with observational data from the NRMN site (LIR).

of the UHI. The data collected from the field measurements during JU2003, combined with data from existing atmospheric observing systems in central Oklahoma, were used in conjunction with numerical modeling.

Numerical model runs were conducted using the uncoupled (HRLDAS–Noah–SLUCM) and coupled (WRF–Noah–SLUCM) models to investigate the sensitivity of T_{2m} and components of the SEB to variations of urban canopy parameters of the SLUCM. The T_{2m} during the day were significantly overestimated and not sensitive to changes in SLUCM parameters, regardless of the PBL scheme used in the WRF Model. Predicted nighttime temperatures decreased in response to a decrease in k_{roof} because of the reduced rate of heat transfer through the roof layer. The T_{2m} were more sensitive to the PBL scheme used in the WRF Model than to changes in SLUCM parameters.

The components of the SEB were more sensitive to SLUCM parameters than T_{2m}. Changes in the Q^* due to changes in α_{roof} were accompanied by compensating changes in Q_H due to increased roof surface heating, consistent with Loridan et al. (2010). Similarly, changes in Q_H due to changes in k_{roof} were accompanied by compensating changes in Q_G. The f_{urb} was the only urban parameter to significantly impact Q_E (Loridan et al. 2010) because Q_E predicted by the SLUCM was erroneously 0 W m^{-2} for the entire period. The f_{urb} simply determined what percentage of Q_E predicted by the Noah LSM contributed to the gridcell value. The fluxes predicted for I/C grid cells showed larger responses to changes to α_{roof}, k_{roof}, and f_{urb} than those predicted for LIR grid cells. The responses of the HRLDAS fluxes to changes in the SLUCM parameters were nearly the same as the responses in the coupled mode. The exception was Q_E, where the response of Q_E to f_{urb} in uncoupled mode

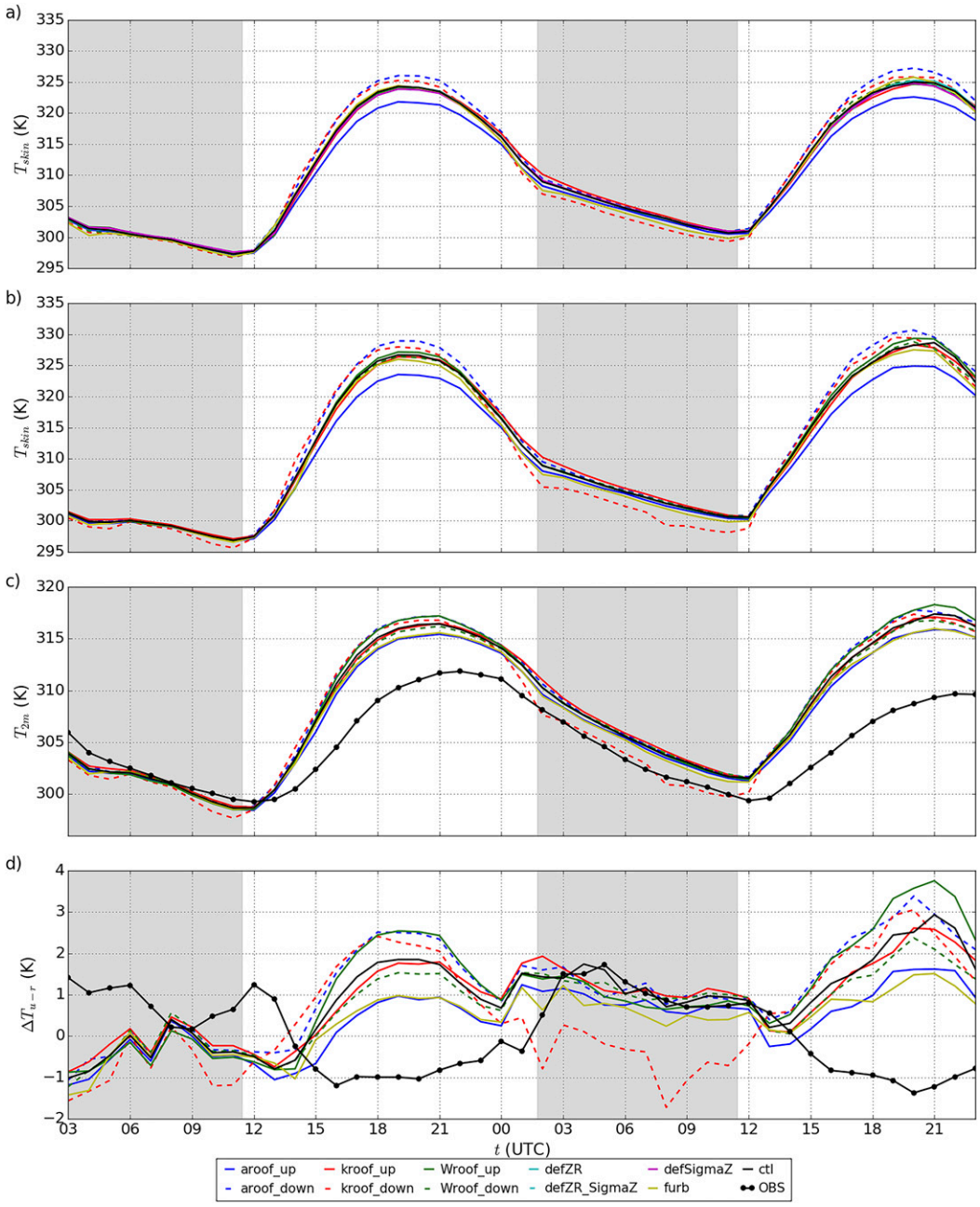

FIG. 13. Diurnal cycles of (a) mean urban skin temperatures, (b) mean urban skin temperatures from implementation of Eq. (6) in the SLUCM, (c) air temperatures at 2 m from implementation of Eq. (6) in the SLUCM, and (d) mean UHI intensity at 2 m from implementation of Eq. (6) in the SLUCM predicted by the WRF Model using the YSU PBL scheme for 14–15 Jul 2003. Observational data from the PNNL HOBO and mesonet sites are shown for comparison.

was less than the response in coupled mode. While the sensitivity to urban parameter variations was similar between the WRF and HRLDAS predictions, the flux magnitudes differed significantly. Thus, it may not be optimal to tune an LSM in uncoupled mode to reproduce observations of the SEB because of potential feedback processes in coupled mode.

Upon examination of T_{skin} predicted by the WRF Model, it was determined that the diagnostic T_{skin} calculated by the SLUCM used the roughness length for grassland instead of a value appropriate for urban land cover. A different, recently proposed method (Li and Bou-Zeid 2014) was used to calculate the T_{skin} within the SLUCM. The results revealed higher values of T_{skin},

especially during the day, and increased sensitivity to the SLUCM parameters. When the new values of T_{skin} were used to calculate the diagnostic T_{2m}, W_{roof} emerged as an additional urban parameter to which T_{2m} was sensitive. Implementing Eq. (6) in the SLUCM increased the sensitivity of T_{2m} to urban canopy parameters, especially during the daytime. However, its implementation worsened the disparity between observed and predicted daytime temperatures, failed to correct the temporal difference, and consequently caused large errors in and unrealistic diurnal cycles of the predicted UHI intensity. These large discrepancies highlight that, while progress in urbanizing weather and climate models has been made, further improvements of these models are needed, additional cases and approaches to calculate T_{skin} should be investigated, and the sensitivity of air temperatures at the surface (2-m level) and also at higher levels should be further analyzed.

Acknowledgments. This study was supported, in part, by funding from National Aeronautics and Space Administration (Award NA17RJ1277); U.S. Department of Defense; and NOAA/Office of Oceanic and Atmospheric Research under NOAA–University of Oklahoma Cooperative Agreement NA11OAR4320072, U.S. Department of Commerce. Some of the computing for this project was performed at the University of Oklahoma Supercomputing Center for Education and Research (OSCER).

REFERENCES

Allwine, K. J., and J. E. Flaherty, 2006: Joint Urban 2003: Study overview and instrument locations. PNNL Tech. Rep. PNNL-15967, 92 pp. [Available online at https://www.pnl.gov/main/publications/external/technical_reports/PNNL-15967.pdf.]

——, J. H. Shinn, G. E. Streit, K. L. Clawson, and M. Brown, 2002: Overview of URBAN 2000: A multiscale field study of dispersion through an urban environment. *Bull. Amer. Meteor. Soc.*, **83**, 521–536, doi:10.1175/1520-0477(2002)083<0521:OOUAMF>2.3.CO;2.

Arnfield, A. J., 2003: Two decades of urban climate research: A review of turbulence, exchange of energy and water, and the urban heat island. *Int. J. Climatol.*, **23**, 1–26, doi:10.1002/joc.859.

ASHRAE, 2009: Material properties. *2009 ASHRAE Handbook: Fundamentals*, American Society of Heating, Refrigerating and Air-Conditioning Engineers, 26.1–26.22.

Au, S. K., and J. L. Beck, 2001: Estimation of small failure probabilities in high dimensions by subset simulation. *Probab. Eng. Mech.*, **16**, 263–277, doi:10.1016/S0266-8920(01)00019-4.

Barlow, J. F., 2014: Progress in observing and modelling the urban boundary layer. *Urban Climate*, **10**, 216–240, doi:10.1016/j.uclim.2014.03.011.

Basara, J. B., and K. C. Crawford, 2002: Linear relationships between root-zone soil moisture and atmospheric processes in the planetary boundary layer. *J. Geophys. Res.*, **107**, 4274, doi:10.1029/2001JD000633.

——, P. K. Hall Jr., A. J. Schroeder, B. G. Illston, and K. L. Nemunaitis, 2008: Diurnal cycle of the Oklahoma City urban heat island. *J. Geophys. Res.*, **113**, D20109, doi:10.1029/2008JD010311.

Beljaars, A. C. M., 1995: The parametrization of surface fluxes in large-scale models under free convection. *Quart. J. Roy. Meteor. Soc.*, **121**, 255–270, doi:10.1002/qj.49712152203.

Best, M. J., 2005: Representing urban areas within operational numerical weather prediction models. *Bound.-Layer Meteor.*, **114**, 91–109, doi:10.1007/s10546-004-4834-5.

——, and C. S. B. Grimmond, 2015: Key conclusions of the First International Urban Land Surface Model Comparison Project. *Bull. Amer. Meteor. Soc.*, **96**, 805–819, doi:10.1175/BAMS-D-14-00122.1.

——, ——, and M. G. Villani, 2006: Evaluation of the urban tile in MOSES using surface energy balance observations. *Bound.-Layer Meteor.*, **118**, 503–525, doi:10.1007/s10546-005-9025-5.

Betts, A. K., F. Chen, K. Mitchell, and Z. Janjić, 1997: Assessment of the land surface and boundary layer models in two operational versions of the NCEP Eta Model using FIFE data. *Mon. Wea. Rev.*, **125**, 2896–2916, doi:10.1175/1520-0493(1997)125<2896:AOTLSA>2.0.CO;2.

Betts, R., and M. J. Best, 2004: Changes in urban temperature and humidity due to radiative forcing, landscape effects and local heat sources. BETWIXT Tech. Briefing Note 6, version 1, 14 pp.

Brock, F. V., K. C. Crawford, R. L. Elliott, G. W. Cuperus, S. J. Stadler, H. L. Johnson, and M. D. Eilts, 1995: The Oklahoma Mesonet: A technical overview. *J. Atmos. Oceanic Technol.*, **12**, 5–19, doi:10.1175/1520-0426(1995)012<0005:TOMATO>2.0.CO;2.

Brotzge, J. A., 2000: Closure of the surface energy budget. Ph.D. dissertation, School of Meteorology, University of Oklahoma, 208 pp.

——, S. J. Richardson, K. C. Crawford, T. W. Horst, F. V. Brock, K. S. Humes, Z. Sorbjan, and R. L. Elliot, 1999: The Oklahoma Atmospheric Surface-layer Instrumentation System (OASIS) Project. *13th Symp. on Boundary Layer and Turbulence*, Dallas, TX, Amer. Meteor. Soc., 612–615.

Burian, S. J., W. S. Han, and M. J. Brown, 2005: Morphological analyses using 3D building databases: Oklahoma City, Oklahoma. Los Alamos National Laboratory Tech. Memo LA-UR-05-1821, 63 pp.

Carter, M., J. M. Shepherd, S. Burian, and I. Jeyachandran, 2012: Integration of lidar data into a coupled mesoscale–land surface model: A theoretical assessment of sensitivity of urban–coastal mesoscale circulations to urban canopy parameters. *J. Atmos. Oceanic Technol.*, **29**, 328–346, doi:10.1175/2011JTECHA1524.1.

Changnon, S. A., and R. G. Semonin, 1978: Chicago Area Program: A major new atmospheric effort. *Bull. Amer. Meteor. Soc.*, **59**, 153–160, doi:10.1175/1520-0477(1978)059<0153:CAPAMN>2.0.CO;2.

——, F. A. Huff, and R. G. Semonin, 1971: METROMEX: An investigation of inadvertent weather modification. *Bull. Amer. Meteor. Soc.*, **52**, 958–967, doi:10.1175/1520-0477(1971)052<0958:MAIOIW>2.0.CO;2.

——, E. Uthe, J. M. Hales, R. R. Braham, and A. H. Auer, 1976: METROMEX update. *Bull. Amer. Meteor. Soc.*, **57**, 304–308, doi:10.1175/1520-0477(1976)057<0304:MU>2.0.CO;2.

Chen, F., and Coauthors, 1996: Modeling of land-surface evaporation by four schemes and comparison with FIFE observations. *J. Geophys. Res.*, **101**, 7251–7268, doi:10.1029/95JD02165.

——, Z. Janjić, and K. Mitchell, 1997: Impact of atmospheric surface-layer parameterizations in the new land-surface scheme of the NCEP mesoscale Eta model. *Bound.-Layer Meteor.*, **85**, 391–421, doi:10.1023/A:1000531001463.

——, M. Tewari, H. Kusaka, and T. T. Warner, 2006: Current status of urban modeling in the community Weather Research and Forecast (WRF) Model. *Sixth Symp. on Urban Environment*, Atlanta, GA, Amer. Meteor. Soc., J1.4. [Available online at https://ams.confex.com/ams/Annual2006/techprogram/paper_98678.htm.]

——, and Coauthors, 2007: Description and evaluation of the characteristics of the NCAR high-resolution land data assimilation system. *J. Appl. Meteor. Climatol.*, **46**, 694–713, doi:10.1175/JAM2463.1.

——, and Coauthors, 2011: The integrated WRF/urban modelling system: Development, evaluation, and applications to urban environmental problems. *Int. J. Climatol.*, **31**, 273–288, doi:10.1002/joc.2158.

Chin, H.-N. S., M. J. Leach, G. A. Sugiyama, J. M. Leone Jr., H. Walker, J. S. Nasstrom, and M. J. Brown, 2005: Evaluation of an urban canopy parameterization in a mesoscale model using VTMX and URBAN 2000 data. *Mon. Wea. Rev.*, **133**, 2043–2068, doi:10.1175/MWR2962.1.

Clawson, K. L., and Coauthors, 2005: Joint Urban 2003 (JU03) SF_6 atmospheric tracer field tests. NOAA Tech. Memo OAR ARL-254, 216 pp. [Available online at http://www.noaa.inel.gov/projects/ju03/docs/Final_JU03.pdf.]

Cosgrove, B. A., and C. J. Alonge, 2008: Application of NARR-based NLDAS ensemble simulations to continental-scale drought monitoring. Preprints, *22nd Conf. on Hydrology*, New Orleans, LA, Amer. Meteor. Soc., 5.3. [Available online at https://ams.confex.com/ams/pdfpapers/134881.pdf.]

——, and Coauthors, 2003: Land surface model spin-up behavior in the North American Land Data Assimilation System (NLDAS). *J. Geophys. Res.*, **108**, 8845, doi:10.1029/2002JD003316.

Doran, J. C., and Coauthors, 1998: The IMADA-AVER boundary layer experiment in the Mexico City area. *Bull. Amer. Meteor. Soc.*, **79**, 2497–2508, doi:10.1175/1520-0477(1998)079<2497:TIABLE>2.0.CO;2.

——, J. D. Fast, and J. Horel, 2002: The VTMX 2000 campaign. *Bull. Amer. Meteor. Soc.*, **83**, 537–551, doi:10.1175/1520-0477(2002)083<0537:TVC>2.3.CO;2.

Dudhia, J., 1989: Numerical study of convection observed during the Winter Monsoon Experiment using a mesoscale two-dimensional model. *J. Atmos. Sci.*, **46**, 3077–3107, doi:10.1175/1520-0469(1989)046<3077:NSOCOD>2.0.CO;2.

——, S.-Y. Hong, and K.-S. Lim, 2008: A new method for representing mixed-phase particle fall speeds in bulk microphysics parameterizations. *J. Meteor. Soc. Japan*, **86A**, 33–44, doi:10.2151/jmsj.86A.33.

Dugway Proving Ground, 2003: Data submission procedures for Joint Urban 2003 database/website. Dugway Proving Ground Meteorology Division Tech. Note 03-90-2, 8 pp.

Dupont, S., T. L. Otte, and J. K. S. Ching, 2004: Simulation of meteorological fields within and above urban and rural canopies with a mesoscale model (MM5). *Bound.-Layer Meteor.*, **113**, 111–158, doi:10.1023/B:BOUN.0000037327.19159.ac.

——, P. G. Mestayer, E. Guilloteau, E. Berthier, and H. Andrieu, 2006: Parameterization of the urban water budget with the Submesoscale Soil Model. *J. Appl. Meteor. Climatol.*, **45**, 624–648, doi:10.1175/JAM2363.1.

Dyer, A. J., and B. B. Hicks, 1970: Flux-gradient relationships in the constant flux layer. *Quart. J. Roy. Meteor. Soc.*, **96**, 715–721, doi:10.1002/qj.49709641012.

Ek, M. B., K. E. Mitchell, Y. Lin, P. Grunmann, E. Rogers, G. Gayno, and V. Koren, 2003: Implementation of the upgraded Noah land surface model in the National Centers for Environmental Prediction operational mesoscale Eta model. *J. Geophys. Res.*, **108**, 8851, doi:10.1029/2002JD003296.

Fan, H., and D. J. Sailor, 2005: Modeling the impacts of anthropogenic heating on the urban climate of Philadelphia: A comparison of the implementations in two PBL schemes. *Atmos. Environ.*, **39**, 73–84, doi:10.1016/j.atmosenv.2004.09.031.

Fast, J. D., J. C. Doran, W. J. Shaw, R. L. Coulter, and T. J. Martin, 2000: The evolution of the boundary layer and its effect on air chemistry in the Phoenix area. *J. Geophys. Res.*, **105**, 22 833–22 848, doi:10.1029/2000JD900289.

——, J. C. Torcolini, and R. Redman, 2005: Pseudovertical temperature profiles and the urban heat island measured by a temperature datalogger network in Phoenix, Arizona. *J. Appl. Meteor.*, **44**, 3–13, doi:10.1175/JAM-2176.1.

Federal Highway Administration, 2013: Mitigation strategies for design exceptions. U.S. Department of Transportation. [Available online at http://safety.fhwa.dot.gov/geometric/pubs/mitigationstrategies/chapter3/3_lanewidth.htm.]

Flagg, D. D., and P. A. Taylor, 2011: Sensitivity of mesoscale model urban boundary layer meteorology to the scale of urban representation. *Atmos. Chem. Phys.*, **11**, 2951–2972, doi:10.5194/acp-11-2951-2011.

Grimmond, C. S. B., and T. R. Oke, 1995: Comparison of heat fluxes from summertime observations in the suburbs of four North American cities. *J. Appl. Meteor.*, **34**, 873–889, doi:10.1175/1520-0450(1995)034<0873:COHFFS>2.0.CO;2.

——, J. A. Salmond, T. R. Oke, B. Offerle, and A. Lemonsu, 2004: Flux and turbulence measurements at a densely built-up site in Marseille: Heat, mass (water and carbon dioxide), and momentum. *J. Geophys. Res.*, **109**, D24101, doi:10.1029/2004JD004936.

——, and Coauthors, 2010: The International Urban Energy Balance Models Comparison Project: First results from phase 1. *J. Appl. Meteor. Climatol.*, **49**, 1268–1292, doi:10.1175/2010JAMC2354.1.

——, and Coauthors, 2011: Initial results from phase 2 of the international urban energy balance model comparison. *Int. J. Climatol.*, **31**, 244–272, doi:10.1002/joc.2227.

Grossman-Clarke, S., J. A. Zehnder, W. L. Stefanov, Y. Liu, and M. A. Zoldak, 2005: Urban modifications in a mesoscale meteorological model and the effects on near-surface variables in an arid metropolitan region. *J. Appl. Meteor.*, **44**, 1281–1297, doi:10.1175/JAM2286.1.

——, ——, T. Loridan, and C. S. Grimmond, 2010: Contribution of land use changes to near-surface air temperatures during recent summer extreme heat events in the Phoenix metropolitan area. *J. Appl. Meteor. Climatol.*, **49**, 1649–1664, doi:10.1175/2010JAMC2362.1.

Halvorson, S. F., D. P. Storwold, and E. M. Vernon, 2006: Joint Urban 2003 database/web design. Preprints, *Sixth Symp. on Urban Environment*, Atlanta, GA, Amer. Meteor. Soc., 5.9a. [Available online at https://ams.confex.com/ams/pdfpapers/99952.pdf.]

Holt, T., and J. Pullen, 2007: Urban canopy modeling in the New York City metropolitan area: A comparison and validation of single- and multilayer parameterizations. *Mon. Wea. Rev.*, **135**, 1906–1930, doi:10.1175/MWR3372.1.

Hong, S.-Y., H.-M. H. Juang, and Q. Zhao, 1998: Implementation of prognostic cloud scheme for a regional spectral model. *Mon. Wea. Rev.*, **126**, 2621–2639, doi:10.1175/1520-0493(1998)126<2621:IOPCSF>2.0.CO;2.

——, J. Dudhia, and S.-H. Chen, 2004: A revised approach to ice microphysical processes for the bulk parameterization of clouds and precipitation. *Mon. Wea. Rev.*, **132**, 103–120, doi:10.1175/1520-0493(2004)132<0103:ARATIM>2.0.CO;2.

——, Y. Noh, and J. Dudhia, 2006: A new vertical diffusion package with an explicit treatment of entrainment processes. *Mon. Wea. Rev.*, **134**, 2318–2341, doi:10.1175/MWR3199.1.

Hu, X.-M., P. M. Klein, M. Xue, J. K. Lundquist, and F. Zhang, 2013a: Impact of low-level jets on the nocturnal urban heat island intensity in Oklahoma City. *J. Appl. Meteor. Climatol.*, **52**, 1779–1802, doi:10.1175/JAMC-D-12-0256.1.

——, ——, and ——, 2013b: Evaluation of the updated YSU planetary boundary layer scheme within WRF for wind resource and air quality assessments. *J. Geophys. Res.*, **118**, 10 490–10 505, doi:10.1002/jgrd.50823.

Janjić, Z. I., 1990: The step-mountain coordinate: Physical package. *Mon. Wea. Rev.*, **118**, 1429–1443, doi:10.1175/1520-0493(1990)118<1429:TSMCPP>2.0.CO;2.

——, 1996: The surface layer in the NCEP Eta Model. Preprints, *11th Conf. on Numerical Weather Prediction*, Norfolk, VA, Amer. Meteor. Soc., 354–355.

——, 2001: Nonsingular implementation of the Mellor-Yamada level 2.5 scheme in the NCEP Meso model. NCEP Office Note 437, 61 pp.

Jiménez, P. A., J. Dudhia, J. F. González-Rouco, J. Navarro, J. P. Montávez, and E. García-Bustamante, 2012: A revised scheme for the WRF surface layer formulation. *Mon. Wea. Rev.*, **140**, 898–918, doi:10.1175/MWR-D-11-00056.1.

Jin, M., J. M. Shepherd, and C. Peters-Lidard, 2007: Development of a parameterization for simulating the urban temperature hazard using satellite observations in climate model. *Nat. Hazards*, **43**, 257–271, doi:10.1007/s11069-007-9117-2.

Kain, J. S., 2004: The Kain–Fritsch convective parameterization: An update. *J. Appl. Meteor.*, **43**, 170–181, doi:10.1175/1520-0450(2004)043<0170:TKCPAU>2.0.CO;2.

Kalanda, B. D., T. R. Oke, and D. L. Spittlehouse, 1980: Suburban energy balance estimates for Vancouver, B.C., using the Bowen ratio–energy balance approach. *J. Appl. Meteor.*, **19**, 791–802, doi:10.1175/1520-0450(1980)019<0791:SEBEFV>2.0.CO;2.

Kim, Y., K. Sartelet, J.-C. Raut, and P. Chazette, 2013: Evaluation of the Weather Research and Forecast/urban model over greater Paris. *Bound.-Layer Meteor.*, **149**, 105–132, doi:10.1007/s10546-013-9838-6.

Kondo, H., Y. Genchi, Y. Kikegawa, Y. Ohashi, H. Yoshikado, and H. Komiyama, 2005: Development of a multi-layer urban canopy model for the analysis of energy consumption in a big city: Structure of the urban canopy model and its basic performance. *Bound.-Layer Meteor.*, **116**, 395–421, doi:10.1007/s10546-005-0905-5.

Koren, V., J. Schaake, K. Mitchell, Q. Duan, F. Chen, and J. Baker, 1999: A parameterization of snowpack and frozen ground intended for NCEP weather and climate models. *J. Geophys. Res.*, **104**, 19 569–19 585, doi:10.1029/1999JD900232.

Kusaka, H., and F. Kimura, 2004a: Coupling a single-layer urban canopy model with a simple atmospheric model: Impact on urban heat island simulation for an idealized case. *J. Meteor. Soc. Japan*, **82**, 67–80, doi:10.2151/jmsj.82.67.

——, and ——, 2004b: Thermal effects of urban canyon structure on the nocturnal heat island: Numerical experiment using a mesoscale model coupled with an urban canopy model. *J. Appl. Meteor.*, **43**, 1899–1910, doi:10.1175/JAM2169.1.

——, H. Kondo, Y. Kikegawa, and F. Kimura, 2001: A simple single-layer urban canopy model for atmospheric models: Comparison with multi-layer and slab models. *Bound.-Layer Meteor.*, **101**, 329–358, doi:10.1023/A:1019207923078.

Landsberg, H. E., 1981: *The Urban Climate.* Academic Press, 275 pp.

Lemonsu, A., C. S. B. Grimmond, and V. Masson, 2004: Modeling the surface energy balance of the core of an old Mediterranean city: Marseille. *J. Appl. Meteor.*, **43**, 312–327, doi:10.1175/1520-0450(2004)043<0312:MTSEBO>2.0.CO;2.

——, S. Belair, and J. Mailhot, 2009: The new Canadian urban modelling system: Evaluation for two cases from the Joint Urban 2003 Oklahoma City Experiment. *Bound.-Layer Meteor.*, **133**, 47–70, doi:10.1007/s10546-009-9414-2.

Li, D., and E. Bou-Zeid, 2013: Synergistic interactions between urban heat islands and heat waves: The impact in cities is larger than the sum of its parts. *J. Appl. Meteor. Climatol.*, **52**, 2051–2064, doi:10.1175/JAMC-D-13-02.1.

——, and ——, 2014: Quality and sensitivity of high-resolution numerical simulation of urban heat islands. *Environ. Res. Lett.*, **9**, 055001, doi:10.1088/1748-9326/9/5/055001.

Lin, C.-Y., F. Chen, J. C. Huang, W.-C. Chen, Y.-A. Liou, W.-N. Chen, and S.-C. Liu, 2008: Urban heat island effect and its impact on boundary layer development and land–sea circulation over northern Taiwan. *Atmos. Environ.*, **42**, 5635–5649, doi:10.1016/j.atmosenv.2008.03.015.

Liu, Y., F. Chen, T. Warner, and J. Basara, 2006: Verification of a mesoscale data-assimilation and forecasting system for the Oklahoma City area during the Joint Urban 2003 field project. *J. Appl. Meteor. Climatol.*, **45**, 912–929, doi:10.1175/JAM2383.1.

Loridan, T., and C. S. B. Grimmond, 2012: Multi-site evaluation of an urban land surface model: Intra-urban heterogeneity, seasonality and parameter complexity requirements. *Quart. J. Roy. Meteor. Soc.*, **138**, 1094–1113, doi:10.1002/qj.963.

——, and Coauthors, 2010: Trade-offs and responsiveness of the single-layer urban canopy parameterization in WRF: An offline evaluation using the MOSCEM optimization algorithm and field observations. *Quart. J. Roy. Meteor. Soc.*, **136**, 997–1019, doi:10.1002/qj.614.

Lowry, W. P., 1974: Project METROMEX: Its history, status, and future. *Bull. Amer. Meteor. Soc.*, **55**, 87–88.

Mailhot, J., and Coauthors, 1998: The Montreal-96 Experiment on Regional Mixing and Ozone (MERMOZ): An overview and some preliminary results. *Bull. Amer. Meteor. Soc.*, **79**, 433–442, doi:10.1175/1520-0477(1998)079<0433:TMEORM>2.0.CO;2.

Margulis, S. A., and D. Entekhabi, 2001: Feedback between the land surface energy balance and atmospheric boundary layer diagnosed through a model and its adjoint. *J. Hydrometeor.*, **2**, 599–620, doi:10.1175/1525-7541(2001)002<0599:FBTLSE>2.0.CO;2.

Martilli, A., 2007: Current research and future challenges in urban mesoscale modelling. *Int. J. Climatol.*, **27**, 1909–1918, doi:10.1002/joc.1620.

——, A. Clappier, and M. W. Rotach, 2002: An urban surface exchange parameterisation for mesoscale models. *Bound.-Layer Meteor.*, **104**, 261–304, doi:10.1023/A:1016099921195.

Masson, V., 2000: A physically-based scheme for the urban energy budget in atmospheric models. *Bound.-Layer Meteor.*, **94**, 357–397, doi:10.1023/A:1002463829265.

——, 2006: Urban surface modeling and the meso-scale impact of cities. *Theor. Appl. Climatol.*, **84**, 35–45, doi:10.1007/s00704-005-0142-3.

——, C. S. B. Grimmond, and T. R. Oke, 2002: Evaluation of the Town Energy Balance (TEB) scheme with direct measurements from dry districts in two cities. *J. Appl. Meteor.*, **41**, 1011–1026, doi:10.1175/1520-0450(2002)041<1011:EOTTEB>2.0.CO;2.

McPherson, R. A., and Coauthors, 2007: Statewide monitoring of the mesoscale environment: A technical update on the Oklahoma Mesonet. *J. Atmos. Oceanic Technol.*, **24**, 301–321, doi:10.1175/JTECH1976.1.

Mellor, G. L., and T. Yamada, 1982: Development of a turbulence closure model for geophysical fluid problems. *Rev. Geophys.*, **20**, 851–875, doi:10.1029/RG020i004p00851.

Mesinger, F., and Coauthors, 2006: North American Regional Reanalysis. *Bull. Amer. Meteor. Soc.*, **87**, 343–360, doi:10.1175/BAMS-87-3-343.

Miao, S., F. Chen, M. A. LeMone, M. Tewari, Q. Li, and Y. Wang, 2009: An observational and modeling study of characteristics of urban heat island and boundary layer structures in Beijing. *J. Appl. Meteor. Climatol.*, **48**, 484–501, doi:10.1175/2008JAMC1909.1.

Mlawer, E. J., S. J. Taubman, P. D. Brown, M. J. Iacono, and S. A. Clough, 1997: Radiative transfer for inhomogeneous atmosphere: RRTM, a validated correlated-k model for the long-wave. *J. Geophys. Res.*, **102**, 16 663–16 682, doi:10.1029/97JD00237.

National Research Council, 2012: *Urban Meteorology: Forecasting, Monitoring, and Meeting Users' Needs.* The National Academies Press, 190 pp., doi:10.17226/13328.

Nemunaitis, K. L., 2014: Observational and model analyses of the Oklahoma City urban heat island. Ph.D. dissertation, School of Meteorology, University of Oklahoma, 223 pp.

NLCD, 2014: Multi-Resolution Land Characteristics Consortium (MRLC). EPA. [Available online at https://www.epa.gov/eco-research/multiresolution-land-characteristics-mrlc-consortium.]

Offerle, B., C. S. B. Grimmond, K. Fortuniak, K. Klysik, and T. R. Oke, 2006: Temporal variations in heat fluxes over a central European city centre. *Theor. Appl. Climatol.*, **84**, 103–115, doi:10.1007/s00704-005-0148-x.

Oke, T. R., 1987: *Boundary Layer Climates.* 2nd ed. Routledge, 435 pp.

——, 1988: The urban energy balance. *Prog. Phys. Geogr.*, **12**, 471–508, doi:10.1177/030913338801200401.

——, and H. A. Cleugh, 1987: Urban heat storage derived as energy balance residuals. *Bound.-Layer Meteor.*, **39**, 233–245, doi:10.1007/BF00116120.

Oleson, K. W., G. B. Bonan, J. Feddema, M. Vertenstein, and C. S. B. Grimmond, 2008: An urban parameterization for a global climate model. Part I: Formulation and evaluation for two cities. *J. Appl. Meteor. Climatol.*, **47**, 1038–1060, doi:10.1175/2007JAMC1597.1.

Otte, T. L., A. Lacser, S. Dupont, and J. K. S. Ching, 2004: Implementation of an urban canopy parameterization in a mesoscale meteorological model. *J. Appl. Meteor.*, **43**, 1648–1665, doi:10.1175/JAM2164.1.

Pan, H.-L., and L. Mahrt, 1987: Interaction between soil hydrology and boundary layer development. *Bound.-Layer Meteor.*, **38**, 185–202, doi:10.1007/BF00121563.

Paulson, C. A., 1970: The mathematical representation of wind speed and temperature profiles in the unstable atmospheric surface layer. *J. Appl. Meteor.*, **9**, 857–861, doi:10.1175/1520-0450(1970)009<0857:TMROWS>2.0.CO;2.

Pinker, R. T., and Coauthors, 2003: Surface radiation budgets in support of the GEWEX Continental Scale International Project (GCIP) and the GEWEX Americas Prediction Project (GAPP), including the North American Land Data Assimilation System (NLDAS) Project. *J. Geophys. Res.*, **108**, 8844, doi:10.1029/2002JD003301.

Roberts, S. M., T. R. Oke, C. S. B. Grimmond, and J. A. Voogt, 2006: Comparison of four methods to estimate urban heat storage. *J. Appl. Meteor. Climatol.*, **45**, 1766–1781, doi:10.1175/JAM2432.1.

Sailor, D. J., and H. Fan, 2002: Modeling the diurnal variability of effective albedo for cities. *Atmos. Environ.*, **36**, 713–725, doi:10.1016/S1352-2310(01)00452-6.

Salamanca, F., A. Martilli, M. Tewari, and F. Chen, 2011: A study of the urban boundary layer using different urban parameterizations and high-resolution urban canopy parameters with WRF. *J. Appl. Meteor. Climatol.*, **50**, 1107–1128, doi:10.1175/2010JAMC2538.1.

Samuelsson, P., B. Bringfelt, and L. P. Graham, 2003: The role of aerodynamic roughness for runoff and snow evaporation in land-surface schemes—Comparison of uncoupled and coupled simulations. *Global Planet. Change*, **38**, 93–99, doi:10.1016/S0921-8181(03)00009-2.

Scott, J. W., Jr., 2006: USGS vector road dataset for Oklahoma County, OK, and vicinity, version 2.0. U.S. Geological Survey, accessed 4 April 2013. [Available online at http://geo.ou.edu/cgi-bin/redesign.cgi?ft=db&template=DataLayer.htm&DataLayersID=69.]

Shafer, M. A., C. A. Fiebrich, D. S. Arndt, S. E. Fredrickson, and T. W. Hughes, 2000: Quality assurance procedures in the Oklahoma Mesonet. *J. Atmos. Oceanic Technol.*, **17**, 474–494, doi:10.1175/1520-0426(2000)017<0474:QAPITO>2.0.CO;2.

Skamarock, W. C., and Coauthors, 2008: A description of the Advanced Research WRF version 3. NCAR Tech. Note NCAR/TN-475+STR, 113 pp., doi:10.5065/D68S4MVH.

Steyn, D. G., J. W. Bottenheim, and R. B. Thomson, 1997: Overview of tropospheric ozone in the Lower Fraser Valley, and the Pacific '93 field study. *Atmos. Environ.*, **31**, 2025–2035, doi:10.1016/S1352-2310(97)00018-6.

Taha, H., 1999: Modifying a mesoscale meteorological model to better incorporate urban heat storage: A bulk-parameterization approach. *J. Appl. Meteor.*, **38**, 466–473, doi:10.1175/1520-0450(1999)038<0466:MAMMMT>2.0.CO;2.

Tewari, M., H. Kusaka, F. Chen, W. J. Coirier, S. Kim, A. A. Wyszogrodzki, and T. T. Warner, 2010: Impact of coupling a microscale computational fluid dynamics model with a mesoscale model on urban scale contaminant transport and dispersion. *Atmos. Res.*, **96**, 656–664, doi:10.1016/j.atmosres.2010.01.006.

Voogt, J. A., and T. R. Oke, 1997: Complete urban surface temperatures. *J. Appl. Meteor.*, **36**, 1117–1132, doi:10.1175/1520-0450(1997)036<1117:CUST>2.0.CO;2.

Vrugt, J. A., H. V. Gupta, L. A. Bastidas, W. Bouten, and S. Sorooshian, 2003: Effective and efficient algorithm for multiobjective optimization of hydrological models. *Water Resour. Res.*, **39**, 1214, doi:10.1029/2002WR001746.

Wang, Z.-H., E. Bou-Zeid, and J. A. Smith, 2011: A spatially-analytical scheme for surface temperatures and conductive heat fluxes in urban canopy models. *Bound.-Layer Meteor.*, **138**, 171–193, doi:10.1007/s10546-010-9552-6.

Webb, E. K., 1970: Profile relationships: The log-linear range and extension to strong stability. *Quart. J. Roy. Meteor. Soc.*, **96**, 67–90, doi:10.1002/qj.49709640708.

Whiteman, C. D., J. M. Hubbe, and W. J. Shaw, 2000: Evaluation of an inexpensive temperature datalogger for meteorological applications. *J. Atmos. Oceanic Technol.*, **17**, 77–81, doi:10.1175/1520-0426(2000)017<0077:EOAITD>2.0.CO;2.

Xia, Y., M. Ek, H. Wei, and J. Meng, 2012: Comparative analysis of relationships between NLDAS-2 forcings and model outputs. *Hydrol. Processes*, **26**, 467–474, doi:10.1002/hyp.8240.

Yap, D., and T. R. Oke, 1974: Sensible heat fluxes over an urban area—Vancouver, B.C. *J. Appl. Meteor.*, **13**, 880–890, doi:10.1175/1520-0450(1974)013<0880:SHFOAU>2.0.CO;2.

Zhang, D.-L., and R. A. Anthes, 1982: A high-resolution model of the planetary boundary layer—Sensitivity tests and comparisons with SESAME-79 data. *J. Appl. Meteor.*, **21**, 1594–1609, doi:10.1175/1520-0450(1982)021<1594:AHRMOT>2.0.CO;2.

——, Y.-X. Shou, R. R. Dickerson, and F. Chen, 2011: Impact of upstream urbanization on the urban heat island effects along the Washington–Baltimore corridor. *J. Appl. Meteor. Climatol.*, **50**, 2012–2029, doi:10.1175/JAMC-D-10-05008.1.